SUPPLEMENTARY MATERIALS

Tools for Overcoming Reliance on Energy-Based Measures in Chemistry: a Tutorial Review

Steven R Kirk* **and Samantha Jenkins***

Key Laboratory of Chemical Biology and Traditional Chinese Medicine Research and Key Laboratory of Resource National and Local Joint Engineering Laboratory for New Petro-chemical Materials and Fine Utilization of Resources, College of Chemistry and Chemical Engineering, Hunan Normal University, Changsha, Hunan 410081, China

email: steven.kirk@cantab.net
email: samanthajsuman@gmail.com

Note, the bold headings below correspond to the titles of the relevant sections of the main text.

1. Supplementary Materials S1. QTAIM bond-path properties; bond-path length (BPL) and the stress tensor $\boldsymbol{\sigma}(\mathbf{r})$.

2. Supplementary Materials S2. Numerical Considerations for Calculation of the Eigenvector-Space Trajectory $\mathsf{T}_i(s)$.

3. Supplementary Materials S3. Intra-molecular Coherent Dynamic Phenomena: The F-NAIBP molecular rotary motor.

4. Supplementary Materials S4. Process for generating eigenvector-directed trajectories for ethane**. Full Symmetry-Breaking and Relevance for Stereochemistry**: Hidden chiral character and steric Effects.

5. Supplementary Materials S5. Full Symmetry-Breaking and Relevance for Stereochemistry: Influence on chiral character of substituents atomic weight.

6. Supplementary Materials S6. Full Symmetry-Breaking and Relevance for Stereochemistry: Electric field induced mixed S and R chiral character.

7. Supplementary Materials S7. Full Symmetry-Breaking and Relevance for Stereochemistry: Why the *cis*-effect is the exception rather than the rule.

1. Supplementary Materials S1. QTAIM bond-path properties; bond-path length (BPL) and the stress tensor **σ**(**r**)

The bond-path length (BPL) is defined as the length of the path traced out by the $\underline{\mathbf{e}}_3$ eigenvector of the Hessian of the total charge density $\rho(\mathbf{r})$, passing through the *BCP*, along which $\rho(\mathbf{r})$ is locally maximal with respect to any neighboring paths. The bond-path curvature separating two bonded nuclei is defined as the dimensionless ratio defined by equation (**S1.1**):

$$\text{(BPL - GBL)/GBL} \qquad \textbf{(S1.1)}$$

where the BPL is defined to be the bond-path length associated and GBL is the inter-nuclear separation. The BPL often exceeds the GBL particularly in strained bonding environments[5]. Earlier, one of the current authors hypothesized that a bond-path may possess 1-D, 2-D or a 3-D morphology[7], with 2-D or a 3-D bond-paths associated with a *BCP* with ellipticity $\varepsilon > 0$, being due to the differing degrees of charge density accumulation, of the λ_2 and λ_1 eigenvalues respectively. Bond-paths possessing zero and non-zero values of the bond-path curvature defined by equation **(2)** can be considered to possess 1-D and 2-D topologies respectively. We start by choosing the length traced out in 3-D by the path swept by the tips of the scaled $\underline{\mathbf{e}}_2$ eigenvectors of the λ_2 eigenvalue, the scaling factor being chosen as the ellipticity ε, see **Scheme S1**.

The quantum stress tensor **σ**(**r**) is directly related to the Ehrenfest force by the virial theorem and therefore provides a physical explanation of the low frequency normal modes that accompany structural rearrangements[8]. In this work we use the definition of the stress tensor proposed by Bader to investigate the stress tensor properties within QTAIM[9]. The quantum stress tensor **σ**(**r**) is used to characterize the mechanics of the forces acting on the electron density distribution in open systems, defined as:

$$\sigma(r) = -\frac{1}{4}\left[\left(\frac{\partial^2}{\partial r_i \partial r_j'} + \frac{\partial^2}{\partial r_i' \partial r_j} - \frac{\partial^2}{\partial r_i \partial r_j} - \frac{\partial^2}{\partial r_i' \partial r_j'}\right) \cdot \gamma(r,r')\right]_{r=r'} \qquad \textbf{(S1.2)}$$

Where $\gamma(\mathbf{r},\mathbf{r}')$ is the one-body density matrix,

$$\gamma(r,r') = N \int \Psi(r,r_2, \ldots ,r_N)\Psi^*(r',r_2, \ldots ,r_N)dr_2 \cdots dr_N \qquad \textbf{(S1.3)}$$

The stress tensor is then any quantity **σ**(**r**), that satisfies equation **(S1.2)** since one can add any divergence-free tensor to the stress tensor without violating this definition.

If we first consider a tiny cube of fluid flowing in 3-D space the stress $\Pi(x, y, z, t)$, a rank-3 tensor field, has nine components [10]: of these the three diagonal components Π_{xx}, Π_{yy}, and Π_{zz} correspond to normal stress. A negative value for these normal components signifies a compression of the cube, conversely a positive value refers to pulling or tension, where more negative/positive values correspond to increased

compression/tension of the cube. Diagonalization of the stress tensor $\boldsymbol{\sigma}(\mathbf{r})$, returns the principal electronic stresses Π_{xx}, Π_{yy}, and Π_{zz} that are realized as the stress tensor eigenvalues $\lambda_{1\boldsymbol{\sigma}}$, $\lambda_{2\boldsymbol{\sigma}}$, $\lambda_{3\boldsymbol{\sigma}}$, with corresponding eigenvectors $\underline{\mathbf{e}}_{1\boldsymbol{\sigma}}$, $\underline{\mathbf{e}}_{2\boldsymbol{\sigma}}$, $\underline{\mathbf{e}}_{3\boldsymbol{\sigma}}$ are calculated within the QTAIM partitioning. The *BCP*s calculated with QTAIM and stress tensor partitionings will not always coincide, particularly under the application of external force, such as an applied torsion.

2. Supplementary Materials S2. Numerical Considerations for Calculation of the Eigenvector-Space Trajectory $\mathsf{T}_i(s)$

Central to the concept of the eigenvector-space trajectory $\mathsf{T}_i(s)$ is the concept of a monotonically increasing sequence parameter ***s***, which may take the form of an increasing integer sequence (0, 1, 2, 3,...) in applications where a set of discrete numbered steps are involved, or a continuous real number. The 3-D eigenvector trajectory $\mathsf{T}_i(s)$ is then defined as an ordered set of points, whose sequence is described by the parameter ***s***. In this application, we used an integer step number for ***s***. We first choose to associate ***s*** = 0 with a specific reference molecular graph, in this case, the energy minimum structure. For a specific *BCP*, the coordinates associated with each of the points are calculated by evaluating the components of the shift vector $\mathbf{dr} = \mathbf{r_b}(s) - \mathbf{r_b}(s\text{-}1)$ where $\mathbf{r_b}$ indicates the location of the *BCP*, from the previous step to the current step in the reference coordinate frame defined by the eigenvectors $\underline{\mathbf{e}}_{1\sigma}, \underline{\mathbf{e}}_{2\sigma}, \underline{\mathbf{e}}_{3\sigma}$.

Note: for displaying the eigenvector trajectories $\mathsf{T}_i(s)$, large steps that can occur at the beginning or end of a $\mathsf{T}_i(s)$ may swamp the appearance of the $\mathsf{T}_i(s)$. To solve this we temporarily filter these steps before including them back in to correctly calculate the U_σ-space stress tensor trajectory $\mathsf{T}_i(s)$.

The calculation of the $\mathsf{T}_i(s)$ is made easier if the code which produces the list of structures corresponding to points along each step of the torsion (CW) and counterclockwise CCW generates these structures at regularly-spaced points. The consequence of this desirable characteristic is that there are few or no large changes or 'spikes' in the magnitude of the *BCP* shift vector **dr** i.e. $\Delta\mathbf{dr}$, between path step s and $s + 1$. Such anomalies occur because some path-following algorithms may employ occasional small predictor-corrector steps that are at least an order of magnitude smaller than standard steps. In this analysis it is observed that such intermittent relatively small steps in turn cause very small shifts **dr** to be interspersed between longer runs of larger changes, causing 'spike' noise in the otherwise smooth trajectories $\mathsf{T}_i(s)$. Such 'spikes', which usually only consist of a single spurious point deviating from the locally smooth stress tensor trajectory, can make potentially large spurious contributions to the stress tensor trajectory $\mathsf{T}_i(s)$ and may be safely filtered. A combination of criteria are recommended for automated rejection of inclusion of a specific point into the trajectories $\mathsf{T}_i(s)$:

1. If the magnitude of the **dr** associated with any current $\mathsf{T}_i(s)$ point is less than 50% of the average of the corresponding **dr** values associated with the immediately preceding point and the immediately following point, the current point is filtered out as a 'spike'.
2. Abrupt changes in direction in the $\mathsf{T}_i(s)$, e.g. turning by more than 60^0 from one $\mathsf{T}_i(s)$ step to the next cause the current point to be labelled as a 'spike'.

These two rules taken together are referred to as the 'turn' filter. These rules can be repeatedly applied across multiple 'passes' through the stress tensor trajectory data as necessary.

It has been observed that the magnitudes of the steps **dr** naturally tend to slowly decrease toward the end of paths, corresponding to a slowed approach to an end minimum, and the corresponding part of the $\mathsf{T}_i(s)$ turns toward the U_i-space origin. A combination of the criteria mentioned above may be deployed to retain these parts of the $\mathsf{T}_i(s)$. An alternative Kolmogorov-Zurbenko[14] data 'smoothing' filter may also be applied - details of the implementation in the QuantVec program '**`trajplot`**', via the '**`avg`**' keyword are given in **Supplementary Materials S4**.

3. Supplementary Materials S3. Intra-molecular Coherent Dynamic Phenomena: The F-NAIBP molecular rotary motor

Non-adiabatic dynamics trajectories for 'fast' and 'slow' paths to the S_0-S_1 conical intersection in the F-NAIBP molecular rotary motor were calculated using a 'custom build' of the TeraChem[15–18] electronic structure code that is not publicly available. Similarly, the generation of the single-point wavefunctions for each step on the dynamics trajectories was performed using a 'custom build' of the Gaussian package that is not publicly available. Scripts for generation of input files, input files generated by these scripts, and all generated single-point molecular graphs, are, however, provided in the accompanying downloadable dataset [https://doi.org/10.5281/zenodo.7830375]. Output **`.log`** files and single-point wavefunctions from the custom code have been omitted from the downloadable dataset as they are very large.

Note: For this case, the single-point wavefunctions were generated as formatted checkpoint (**`.fchk`**) files compatible with AIMAll (which AIMALL converts first to **`.wfx`** format). These formatted checkpoint files are, to our knowledge, only output by the Gaussian electronic structure code. A few electronic structure codes can, however, produce compatible **`.wfx`** files directly and many electronic structure codes can also produce Molden-format wavefunction outputs which can be converted to **`.wfx`** format using the freely-available open-source code 'Molden2AIM' [19].

This dataset demonstrates how, for an eigenvector-following NG-QTAIM calculation for dynamics, sequences of single-point wavefunctions produced by other codes can be used and converted to sequences of molecular graphs. Once a time-ordered dynamics sequence of molecular graph **`.sumviz`** files were obtained, further analysis was performed according to the procedure for trajectory generation outlined in **Supplementary Materials S4**.

The NAMD simulations of the chemically modified molecular motors of the F-NAIBP molecular rotary motor were demonstrated, see the **Supplementary Materials S2** for further explanation of quantities used. Earlier, scalar QTAIM determined that torsional motion of the selected dynamics trajectory (F-NAIBP) molecular motor[20] blades was controlled by unusually strongly coupled "sticky" F--H *BCP* intramolecular bond-paths between atoms of the rotor and stator blades[21]. The "sticky" F--H *BCP* were present only for the slow dynamics trajectory, the stickiness was again caused by a degree of covalent character in the F--H *BCP* on the basis of values of $H(\mathbf{r_b}) < 0$.

The stress tensor trajectories $\mathsf{T}_{\boldsymbol{\sigma}}(s)$ associated with the S_0 and S_1 electronic states were found to occupy separate and distinct regions at the conical intersection (C.I.)[22] due to the use of the symmetry-breaking $\mathsf{U}_{\boldsymbol{\sigma}}$-space[23] that create separations associated with the S_1 compared with the S_0 state.

The morphology of the $\mathsf{T}_{\boldsymbol{\sigma}}(s)$ associated with the fast non-adiabatic dynamics trajectory was relatively

isotropic with evenly spaced $\mathsf{T}_{\sigma}(s)$ steps with a small $\boldsymbol{t}_{3\mathbf{max}} = (\underline{\mathbf{e}}_{3\sigma}\cdot\mathbf{dr})_{\mathbf{max}}$ component corresponding to motion along the axial C1-C2 *BCP* bond-path.

Table S3. A summary of the stress tensor trajectory $\mathsf{T}_{\sigma}(s)$ for the reaction pathways (S_1) leading to the hop events at the conical intersections (CI) of the fast and slow dynamics trajectories for the F-NAIBP motor for the C1-C2-*BCP*. The duration, $Time^{CI}$ in femtoseconds (fs), from the start of the fast and slow dynamics trajectories to the respective $\mathsf{T}_{\sigma}(s)^{CI}$, corresponding real space separation l^{CI}_{S0}, l^{CI}_{S1} and stress tensor trajectory space separation $\mathsf{L}_{\sigma}{}^{CI}_{S0}$, $\mathsf{L}_{\sigma}{}^{CI}_{S1}$, in a.u, and the locations in U_{σ}-space, $\{\boldsymbol{t}_1, \boldsymbol{t}_2, \boldsymbol{t}_3\}^{CI}_{S0}$ and $\{\boldsymbol{t}_1, \boldsymbol{t}_2, \boldsymbol{t}_3\}^{CI}_{S1}$ corresponding to the S_1 and S_0 states respectively, see **Figure 2** (Top).

$Time^{CI}$	l^{CI}_{S0} l^{CI}_{S1}	$\mathsf{L}_{\sigma}{}^{CI}_{S0}$	$\mathsf{L}_{\sigma}{}^{CI}_{S1}$	$\{\boldsymbol{t}_1, \boldsymbol{t}_2, \boldsymbol{t}_3\}^{CI}_{S0}$	$\{\boldsymbol{t}_1, \boldsymbol{t}_2, \boldsymbol{t}_3\}^{CI}_{S1}$
			Fast		
352	3.387	3.405	0.948	0.964	{(-0.0042),(0.0184),(-0.0009)}	{(-0.0047),(0.0177),(-0.0006}
			Slow		
574	5.341	5.342	1.626	1.642	{(0.0198),(0.0033),(0.0138)}	{(0.0225), (0.0052), (0.0149)}

4. Supplementary Materials S4. Process for generating eigenvector-directed trajectories for ethane**. Full Symmetry-Breaking and Relevance for Stereochemistry**: Hidden chiral character and steric Effects.

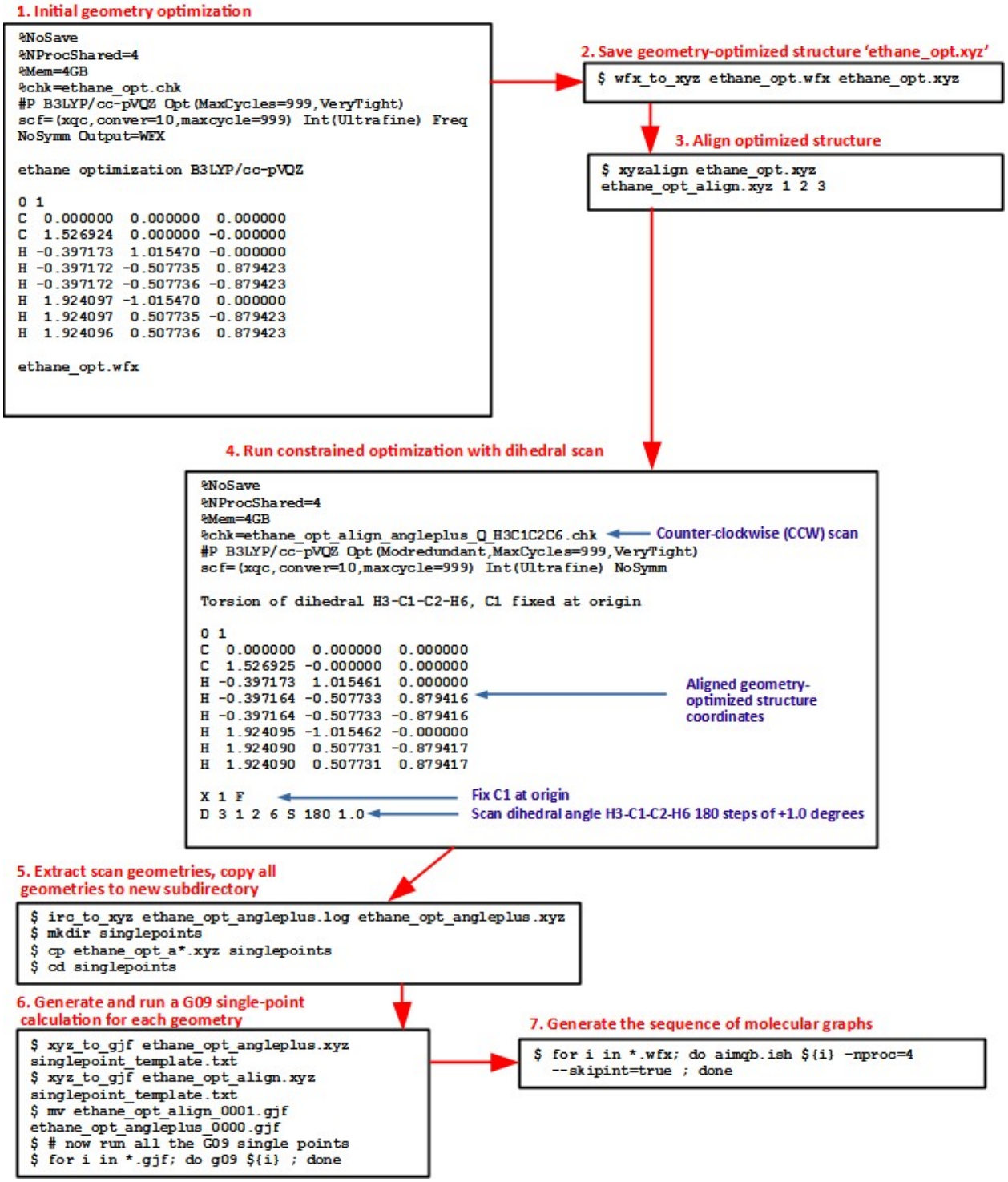

Figure S4. Process for generating eigenvector-directed trajectories for generation of the eigenvector-directed trajectory $T_{\sigma D}(s)$ of the H3-C1-C2-H6 dihedral angle that corresponds to the $\mathbf{Q}_{\sigma}$ isomer of ethane, using the archived data files specified in this section.

The walkthrough in **Figure S4** can be used to generate the $T_{\sigma D}(s)$ of the H3-C1-C2-H6 dihedral angle

corresponding to the $\mathbf{Q}_{\sigma}$ isomer of ethane uses the Gaussian (G09) electronic structure code, some QuantVec programs and the QTAIM code AIMAll. An additional visualization tool such as GaussView or Avogadro (https://avogadro.cc/) is also useful. The description of the calculation process assumes that all of the mentioned QuantVec Python codes mentioned below, along with their dependencies, have been previously installed into the user's Python environment, using, e.g. the **'pip'** Python package manager. It also assumes the use of a '**bash**'-compatible shell with output redirection, pipes and Unix commands such as '**mkdir**', '**ls**', '**tee**' and '**grep**' available. MS Windows users can obtain a '**bash**' shell by using BusyBox [https://busybox.net/] or Cygwin [https://www.cygwin.com/].

In the description below, command lines for a '**bash**'-shell command line are shown prefixed by the '**$**' character. The numbered sections below refer to the corresponding boxes in Figure S4. File names, directories, commands and command-line parameters are shown in the **Courier New** ('typewriter-style') font. The corresponding data files are available for download at: https://doi.org/10.5281/zenodo.7824035

1. Initial geometry optimization

Using G09, geometry-optimize the molecular geometry of ethene. Additionally, generate a **.wfx** file for the optimized geometry (see the G09 input file **ethane_opt.gjf**)

2. Save geometry-optimized structure 'ethane_opt.xyz'

Once Step 1 has completed and one has checked that the resulting structure is a local energy minimum (i.e. no imaginary frequencies in the Gaussian output), one can either extract the optimized coordinates in **.xyz** format by loading the Gaussian output file into either GaussView or Avogadro (https://avogadro.cc/) and exporting the final coordinates, or converting the **.wfx** file back into **.xyz** form using the QuantVec program '**wfx_to_xyz**':

```
$ wfx_to_xyz ethane_opt.wfx ethane_opt.xyz
```

3. Align optimized structure

Using the '**xyzalign**' program within QuantVec to rotate the optimized molecule so as to 1) move the C1 atom to the coordinate origin, 2) Align the C1-C2 bond along the x-axis, then 3) additionally align the molecule so that it lies in the x-y plane.

```
$ xyzalign ethane_opt.xyz ethane_opt_aligned.xyz 1 2 3
```

4. Run constrained optimization with dihedral scan

Run a constrained optimization, scanning the specified dihedral angle parameter, using the aligned geometry-optimized structure in **ethane_opt_align.xyz** as a starting point. Atom C1 is constrained to stay at the coordinate origin and the dihedral angle is scanned in steps of +1.0 degree, for 180 steps. The **.log** file produced by G09 when the scan is completed contains the full details of the progress of the constrained optimization scan.

Do two such constrained optimization scans: one where the angle step is +1.0 degrees and another where the angle step is -1.0 degrees: the corresponding input files are provided in the data set at https://doi.org/10.5281/zenodo.7824035, for the dihedral angle H3-C1-C2-H6.

(see G09 input files: **ethane_opt_angleplus.gjf** [angle step = +1.0 degrees case, counter-clockwise (CCW)]) and **ethane_opt_angleminus.gjf** [angle step = -1.0 degrees case, clockwise (CW)])

5. Extract scan geometries, copy all geometries to new subdirectory

Extract a multi-step **.xyz** file containing the atomic coordinates at every step in the dihedral angle scan using the '**irc_to_xyz**' QuantVec command.

Make a new subdirectory '**singlepoints**' and move the **ethane_opt_angleplus.xyz** and **ethane_opt_align.xyz** files there.

```
$ irc_to_xyz ethane_opt_angleplus.log ethane_opt_angleplus.xyz
$ mkdir singlepoints
$ cp ethane_opt_a*.xyz singlepoints
$ cd singlepoints
```

6. Generate and run a G09 single-point calculation for each geometry

In the '**singlepoints**' subdirectory, convert every intermediate geometry held in the multi-step **.xyz** file into a single-point G09 calculation of the wavefunction using **xyz_to_gjf**, saving the wavefunction details to a **.wfx**-format output file. This will generate G09 input files for every structure in the scan: these will be numbered 0001, 0002 etc. Also, generate a single point wavefunction calculation for the starting aligned structure **ethane_opt_align.xyz** file as **ethane_opt_angleplus_0000.gjf**, as this is the 'zero torsion angle' case. Run all the newly-created **.gjf** Gaussian single-point input files with G09. Once all these **.gjf** files have been run with G09, each should have produced a corresponding **.WFX** file

containing the single-point converged wavefunction.

```
$ xyz_to_gjf ethane_opt_angleplus.xyz singlepoint_template.txt
$ xyz_to_gjf ethane_opt_aligned.xyz singlepoint_template.txt
$ mv ethane_opt_aligned_0001.gjf ethane_opt_angleplus_0000.gjf
$ for i in *.gjf; do g09 ${i} ; done
```

7. Generate the sequence of molecular graphs

In the '**singlepoints**' subdirectory, run AIMAll on each of the **.wfx** files to generate one **.sumviz** file (containing molecular graph data) for each **.wfx** file. The **aimqb.ish** command line parameters given will speed up the calculations: **--nproc** sets the number of execution threads and **--skipint=true** avoids atomic integrations, which are not needed here. The result will be a set of **.sumviz** files, each containing a molecular graph, which is used as an input sequence for construction of an NG-QTAIM trajectory.

```
$ for i in *.wfx; do aimqb.ish ${i} --nproc=4 --skipint=true ; done
```

Procedure for generation of a trajectory from a list of .sumviz files (molecular graphs)

I. Make a specific directory to hold the **.sumviz** files previously created for this trajectory. Copy all the relevant **.sumviz** files into this newly-created directory, then make this directory your current directory, e.g.

```
mkdir trajectory; cp *.sumviz trajectory/ ; cd trajectory/
```

II. Create a text file containing an ordered list of the names of the **.sumviz** files previously created for this trajectory, one name per line, using the command:

```
ls -1 *.sumviz > sumviz_filelist.txt
```

This make a text file '**sumviz_filelist.txt**' with a list of **.sumviz** filenames that looks like:

```
ethane_opt_align_angleplus_0000.sumviz
ethane_opt_align_angleplus_0001.sumviz
```

…

and so on.

III. Run the projection code '**drproject3**' (interactive), sending the output both to the screen and a text

file to capture the output for further processing using the '**tee**' command.

```
drproject3 sumviz_filelist.txt | tee ethane_angleplus_drproject.txt
```

The **drproject3** program will then open the file list you provided, and load all of the **.sumviz** files mentioned, in order, therein. A count of the loaded **.sumviz** files is shown, and then the program prompts for its first interactive input from the user, e.g.

```
Do you want to define a new origin of coordinates?
1: No - use existing origin
2: Yes - use an atomic position as new origin, extra atomic positions to define frame

Enter choice or 99 to go back/exit: 1
```

Usually (and in this case), we do not want to redefine the origin of coordinates, so we type '**1**' and press the Return key. The program prints confirmation of this choice, and then allows selection of a subset of critical points, e.g. bond critical points (BCPs). Option 3 is the usual choice:

```
Using conventional origin and axes - no additional alignment
Select a subset of CPs for analysis
1: Closed shell BCPs
2: Shared shell BCPs
3: All BCPs
4: All NACPs
5: All RCPs
6: All CCPs
7: All CPs

Enter choice or 99 to go back/exit: 3
```

The program confirms this choice, shows the names of the first and last **.sumviz** file (which hold the molecular graph data) names, then asks the user which **.sumviz** file should be used to provide the reference eigenvectors, e.g.

```
Selected all BCPs

First file in input list: ethane_opt_align_angleplus_0000.sumviz
Last file in input list : ethane_opt_align_angleplus_0181.sumviz
Which file from the input list should be used for projection axes?
1: First file in the input list - ethane_opt_align_angleplus_0000.sumviz
2: Last file in the input list - ethane_opt_align_angleplus_0181.sumviz
3: File from specific numbered position in the list (0=first file)
```

```
4: Previous file in the input list (tracking)

Enter choice or 99 to go back/exit: 1
```

The reference for the projection axes is taken in our analysis to be the **first** file in the input list (option 1). The reference can, in general, correspond to the starting point in a time series, or another sensible reference point in the sequence (e.g. in the case of tracking down an intrinsic reaction coordinate (IRC) path in a molecule, from a transition state to a local minimum on the potential energy surface, the **first** file is also chosen as it will correspond to the transition state molecular graph and the last file will correspond to the local energy minimum at the end of the IRC path). Additionally, the program provides the ability to use a **different** set of reference (projection) eigenvectors in each trajectory step, using option '4'. In this 'tracking' mode, at each step (i.e. calculating a CP shift between step **s-1** and step **s**), the reference (projection) eigenvectors are taken from the molecular graph for step **s-1**, rather than a specific position in the file list. This extra 'tracking' mode has never been used in our work to date, but is reserved for future use.

The program then proceeds to construct the step-by-step projections of the critical point shifts onto the reference eigenvectors, outputting these projections (and the magnitude of the shift '**moddr**') for both the standard Hessian $\rho(\mathbf{r})$ eigenvectors and the stress tensor eigenvectors for each selected type of critical point in the molecular graph (the output can be found in **angleplus/singlepoints/trajectory/more ethane_angleplus_drproject.txt**).

The projections are calculated for each recognised BCP. **Note**: it can occasionally occur that the labelled identities of critical points can change during a sequence of molecular graphs. The program relies on the labelled identity of the critical points staying the same across all the **.sumviz** files. In situations where a CP vanishes between one molecular graph and the next molecular graph in the sequence, or when a previously nonexistent CP suddenly appears, the program will pause and ask the user what to do. Provided options include: a) treating the new labelled CP as if it is actually just a renamed version of the same physical CP that appears under a different name in the previous molecular graph: in this case, the user is prompted to identify its 'old' name, or b) ignoring this CP for the rest of the sequence.

IV(i). The trajectory information for a specific chosen CP can then be filtered out of the output file from '**drproject3**'. We want obtain the trajectory for BCP C1-C2:

```
grep ' C1-C2 ' ethane_angleplus_drproject.txt > ethane_angleplus_drproject_C1-C2.txt
```

Note the spaces (essential!) on either side of the BCP name in the search expression for the '**grep**' command.

IV(ii). An optional supplementary 'denoising' step may be needed for the trajectory data at this point in the process. We have previously found that in the case of a trajectory derived from an IRC pathway, that the change in CP position can be anomalously large relative to the other steps at the beginning and end of the trajectory. In this case, this is due to the IRC tracking algorithm implementation used in the accompanying electronic structure code. In our previous work, the magnitude of the first step down the IRC path away from a properly-converged transition state was not controllable, unlike the magnitude of subsequent steps for which a maximum magnitude could be specified. Similarly, IRC algorithms tend not to go all the way to the 'end' energy local minimum, so that the CP shift associated with the last IRC step is considerably smaller than the CP shift calculated from the IRC endpoint to the actual separately-converged local energy minimum produced by geometry optimization. This effect, where the first and last CP shifts are anomalously large relative to the other CP shifts, also occurs in eigenvector-directed trajectories for constrained torsional scans. Hence, we always ignore the first and last step of calculated trajectories: see the later section on 'Denoising trajectories' for further details.

V. The trajectory can then be plotted for visual inspection, and calculation of the 'bounding box' dimensions $\{t_{1max}, t_{2max}, t_{3max}\}$, using the program '**trajplot**'. Input for '**trajplot**' is self-documenting (see the file **angleplus/singlepoints/trajectory/trajplot_in.txt**).

The program is run thus:

```
trajplot trajplot_in.txt --matrix stress --modulus no
```

The '**trajplot**' program loads each named trajectory data file specified in the '**trajplot**' input file in turn, first applying any requested noise filtering operations, then drawing each trajectory on the screen in a 3-D interactive rotatable plot using the line and symbol attributes specified. If CSV-format (Comma-Separated Variable: easily importable into visualization tools, plotting packages and spreadsheets) output has been selected, each filtered trajectory is output to a separate named CSV file for future analysis or plotting. Bitmap images of user-created plots may also be saved (in several widely-used image data formats) from within the '**trajplot**' program. Additionally, '**trajplot**' prints information about the 'bounding box' values for each filtered trajectory. The full list of command-line options is accessible using the **--**

help command line parameter:

```
trajplot --help
```

Optional: 'Denoising' trajectories

It is sometimes required to pre-screen the extracted CP trajectory data for 'transient' noise, which can appear on the first and last line of the output file from **4**. above, but which can also appear elsewhere in the trajectory. A convenient way to check the trajectory for such transients in trajectory data is to use the command:

```
screentraj mytrajectory_drproject_C1-C2.txt
```

This opens a graphical window (using the Matplotlib library [24]) showing the dependence of the modulus of each BCP shift (y-axis) on the step number(x-axis). Trajectory steps which have a very large modulus relative to immediately preceding or subsequent steps, showing up as large 'one-point' deviations from the locally smooth variation of the modulus from one step to the next, are an artefact of the convergence behaviour of the underlying electronic structure code. Hovering the mouse pointer over any transient points allows identification of the specific 'noisy' points. These transient points can then be manually filtered out by 'commenting out', using a text editor, the corresponding lines in the BCP trajectory data using a leading '#' character. We **always** comment out at least the first and last line of these trajectory files, as the corresponding steps very frequently have spuriously large values in the final ('**moddr**') column relative to the nearby points, regardless of the physical system or the details of how the sequence of **.sumviz** files has been created. What should remain after this pre-screening process is a relatively smooth dependence on the shift modulus with trajectory step.

The available filters for numerical noise in '**trajplot**' are '**none**' (i.e. does not change the data), '**turn**', which rejects points where the trajectory turns by more than a specific threshold angle, and '**avg**' which 'smooths' the trajectory using an averaging procedure on pairs of successive trajectory points - these filter procedures are described in S1. The most frequently used filters are '**none**' and '**avg**'. The '**trajplot**' program displays information about any denoising operations that are used.

The presence of large chirality C_σ values for the D_{4128} and D_{5127} isomers created from the torsional dihedral angles H4-C1-C2-H8 and H5-C1-C2-H7 respectively, demonstrated asymmetry in the CCW vs CW torsion for the C1-C2 *BCP*, i.e. relating to steric effects in U_σ-space, see the numbering scheme in **Figure 3** (Top) of

ethane in the main text. The chirality $\mathsf{C}_{\boldsymbol{\sigma}}$ values for the D_{4128} and D_{5127} isomers that possess equal magnitude but opposite signs which is consistent with equal and opposite torsions of the ethane CH_3 groups located in a staggered configuration either side of the torsional C1-C2 *BCP* bond-path. The chirality $\mathsf{C}_{\boldsymbol{\sigma}}$ values of the D_{4128} and D_{5127} isomers were two orders of magnitude greater than the corresponding values of the bond-axiality $\mathsf{B}_{\boldsymbol{\sigma}}$ thus indicated the dominance of steric effects over hyper-conjugation in $\mathsf{U}_{\boldsymbol{\sigma}}$-space interpretation. Using all nine dihedral angles yielded three symmetry inequivalent $\mathsf{T}_{\boldsymbol{\sigma}}(s)$: the $\mathbf{Q}_{\boldsymbol{\sigma}}$ isomer $\mathbf{S}_{\boldsymbol{\sigma}}$ and $\mathbf{R}_{\boldsymbol{\sigma}}$ stereoisomers. The variation of the ethane C1-C2 *BCP* ellipticity ε for the CW and CCW torsions for the D_{3126} isomer, torsional dihedral angle H3-C1-C2-H6, displays mirror symmetry at $\theta = 0.0^{o}$ with chirality $\mathsf{C}_{\boldsymbol{\sigma}}$ assignment $\mathbf{Q}_{\boldsymbol{\sigma}}$. The $\mathbf{Q}_{\boldsymbol{\sigma}}$ isomer is the 'null-isomer' that identifies ethane as achiral in $\mathsf{U}_{\boldsymbol{\sigma}}$-space since $\mathsf{C}_{helicity} = 0$, see **Figure 3** of the main text and **Table S4(a-b)**.

Table S4(a). The maximum stress tensor projections $\{t_{1max}, t_{2max}, t_{3max}\}$ of the dominant torsional C1-C2 *BCP* for ethane; all entries have been multiplied by 10^3, see the **Supplementary Materials S2** for further explanation of quantities used.

$\{t_{1max}, t_{2\,max}, t_{3max}\}$

	CW	**CCW**
3126	{0.771252,0.748155,0.697967}	{0.771166,0.748182,0.697964}
3127	{0.459897,0.763783,0.700097}	{0.764206,0.880854,0.696895}
3128	{0.764193,0.880798,0.696914}	{0.459836,0.763691,0.700077}
4126	{0.781696,0.770840,0.697358}	{0.770459,0.741005,0.699078}
4127	{0.482438,0.801677,0.698794}	{0.777752,0.867005,0.697808}
4128	{0.767348,0.895447,0.699182}	{0.476248,0.769004,0.698245}
5126	{0.770459,0.741110,0.699058}	{0.781664,0.770948,0.697358}
5127	{0.476229,0.769069,0.698236}	{0.767185,0.895420,0.699221}
5128	{0.777567,0.868016,0.697825}	{0.482479,0.801824,0.698811}

Table S4(b). The torsion C1-C2 *BCP* of the symmetry inequivalent U_σ-space distortion sets $\{C_\sigma,F_\sigma,B_\sigma\}$, the sum $\sum\{C_\sigma,F_\sigma,B_\sigma\}$ and the chirality-helicity function $C_{helicity}$ with the total chirality C_σ and B_σ chirality assignments denoted by $\mathbf{[C_\sigma,B_\sigma]}$. The four-digit sequence in the left column refers to the atom numbering used in the dihedral angles (D_{3126} = H3-C1-C2-H6, D_{4128} = H4-C1-C2-H8, D_{5127} = H5-C1-C2-H7) used to construct the stress tensor trajectories $T_\sigma(s)$, see **Table S4(a)** and **Figure 3** (Top) of the main text. The $C_{helicity}$ = (chirality C_σ)×(axiality B_σ) = $C_\sigma B_\sigma$. The classification $\mathbf{[C_\sigma,B_\sigma]}$ is $\mathbf{Q_\sigma}$ when the $\sum C_{helicity} = 0$.

Isomer	$\{C_\sigma,F_\sigma,B_\sigma\}$	$C_{helicity}$	$\mathbf{[C_\sigma,B_\sigma]}$
D_{3126}	{-0.00010$\mathbf{[R_\sigma]}$,0.00003$\mathbf{[S_\sigma]}$,-0.000003$\mathbf{[R_\sigma]}$}	0	$\mathbf{[Q_\sigma]}$
D_{4128}	{-0.29110$\mathbf{[R_\sigma]}$,-0.12644$\mathbf{[R_\sigma]}$,-0.00094$\mathbf{[R_\sigma]}$}	-0.0003	$\mathbf{[R_\sigma,R_\sigma]}$
D_{5127}	{ 0.29096$\mathbf{[S_\sigma]}$, 0.12635$\mathbf{[S_\sigma]}$, 0.00099$\mathbf{[S_\sigma]}$}	0.0003	$\mathbf{[S_\sigma,S_\sigma]}$

$\sum\{C_\sigma,F_\sigma,B_\sigma\}$	$\sum C_{helicity}$	
{-0.00024$\mathbf{[R_\sigma]}$,-0.00006$\mathbf{[R_\sigma]}$,0.000047$\mathbf{[S_\sigma]}$}	0	$\mathbf{[Q_\sigma]}$

5. Supplementary Materials S5. Full Symmetry-Breaking and Relevance for Stereochemistry: Influence on chiral character of substituents atomic weight.

Gaussian input files are listed below for geometry-optimization and constrained optimization with dihedral angle scanning are listed below. Only the input files for dihedral angle scanning for the 3-1-2-6 dihedral angle with steps of +1.0 degrees are listed - the corresponding files for scanning with steps of -1.0 degrees and the other possible dihedral angles are omitted for brevity. These are identical except that a) the last number on the last line (beginning with 'D') should be -1.0 rather than 1.0 and b) the atom numbers defining the dihedral, i.e. appearing immediately after the 'D', are modified accordingly.

Singly-substituted ethane - F

- Optimization

```
%NoSave
%NProcShared=4
%Mem=4GB
%chk=ethane_F_start.chk
#P B3LYP/cc-pVQZ Opt(MaxCycles=999,VeryTight) scf=(xqc,conver=10,maxcycle=999)
Int(Ultrafine) NoSymm Output=wfx

Geometry optimization: ethane-F

0 1
C  0.000000  0.000000  0.000000
C  1.526925 -0.000000  0.000000
F -0.397173  1.015461  0.000000
H -0.397164 -0.507733  0.879416
H -0.397164 -0.507733 -0.879416
H  1.924095 -1.015462 -0.000000
H  1.924090  0.507731 -0.879417
H  1.924090  0.507731  0.879417

ethane_F_opt.wfx
```

- Dihedral angle scan of optimized structure with steps of +1.0 degrees

```
%NoSave
%NProcShared=4
%Mem=4GB
%chk=ethane_F_3126_angleplus.chk
#P B3LYP/cc-pVQZ Opt(Modredundant,MaxCycles=999,VeryTight)
scf=(xqc,conver=10,maxcycle=999) Int(Ultrafine) NoSymm

Dihedral scan 3-1-2-6 step +1.0

0 1
C  0.000000  0.000000  0.000000
C  1.509755  0.000000  0.000000
F -0.478649  1.314795  0.000000
H -0.405025 -0.488568  0.887329
H -0.405025 -0.488568 -0.887329
H  1.880223 -1.026118  0.000000
H  1.896250  0.504083 -0.884763
H  1.896250  0.504083  0.884763

X 1 F
```

```
D 3 1 2 6 S 180 1.0
```

Singly-substituted ethane - Cl

- Optimization

```
%NoSave
%NProcShared=4
%Mem=4GB
%chk=ethane_Cl_start.chk
#P B3LYP/cc-pVQZ Opt(MaxCycles=999,VeryTight) scf=(xqc,conver=10,maxcycle=999)
Int(Ultrafine) NoSymm Output=wfx

Geometry optimization: ethane-Cl

0 1
C  0.000000  0.000000  0.000000
C  1.526925 -0.000000  0.000000
Cl -0.397173  1.015461  0.000000
H -0.397164 -0.507733  0.879416
H -0.397164 -0.507733 -0.879416
H  1.924095 -1.015462 -0.000000
H  1.924090  0.507731 -0.879417
H  1.924090  0.507731  0.879417

ethane_Cl_opt.wfx
```

- Dihedral angle scan of optimized structure with steps of +1.0 degrees

```
%NoSave
%NProcShared=4
%Mem=4GB
%chk=ethane_cl_3126_angleminus.chk
#P B3LYP/cc-pVQZ Opt(Modredundant,MaxCycles=999,VeryTight)
scf=(xqc,conver=10,maxcycle=999) Int(Ultrafine) NoSymm

Dihedral scan 3-1-2-6 step +1.0

0 1
C  0.000000  0.000000  0.000000
C  1.512864  0.000000  0.000000
Cl -0.667468  1.687459 -0.000000
H -0.409142 -0.479160  0.884193
H -0.409142 -0.479160 -0.884193
H  1.874694 -1.030209  0.000000
H  1.905794  0.500624 -0.883024
H  1.905794  0.500624  0.883024

X 1 F
D 3 1 2 6 S 180 1.0
```

Singly substituted ethane - Br

- Optimization

```
%NoSave
%NProcShared=4
%Mem=4GB
%chk=ethane_Br_start.chk
```

```
#P B3LYP/cc-pVQZ Opt(MaxCycles=999,VeryTight) scf=(xqc,conver=10,maxcycle=999)
Int(Ultrafine) NoSymm Output=wfx

Geometry optimization: ethane-Br

0 1
C  0.000000  0.000000  0.000000
C  1.526925 -0.000000  0.000000
Br -0.397173  1.015461  0.000000
H -0.397164 -0.507733  0.879416
H -0.397164 -0.507733 -0.879416
H  1.924095 -1.015462 -0.000000
H  1.924090  0.507731 -0.879417
H  1.924090  0.507731  0.879417

ethane_Br_opt.wfx
```

- Dihedral angle scan of optimized structure with steps of +1.0 degrees

```
%NoSave
%NProcShared=4
%Mem=4GB
%chk=ethane_Br_3126_angleplus.chk
#P B3LYP/cc-pVQZ Opt(Modredundant,MaxCycles=999,VeryTight)
scf=(xqc,conver=10,maxcycle=999) Int(Ultrafine) NoSymm

Dihedral scan 3-1-2-6 step +1.0

0 1
C  0.000000  0.000000  0.000000
C  1.511699  0.000000  0.000000
Br -0.735505  1.836989  0.000000
H -0.417703 -0.466329  0.885526
H -0.417703 -0.466329 -0.885526
H  1.870418 -1.032082 -0.000000
H  1.908635  0.497731 -0.882687
H  1.908635  0.497731  0.882687

X 1 F
D 3 1 2 6 S 180 1.0
```

Doubly-substituted ethane - Cl,F, geometric stereoisomer = 'R'

- Optimization

```
%NoSave
%NProcShared=4
%Mem=4GB
%chk=ethane_3Cl5F_R_start.chk
#P B3LYP/cc-pVQZ Opt(MaxCycles=999,VeryTight) scf=(xqc,conver=10,maxcycle=999)
Int(Ultrafine) NoSymm Output=wfx

Geometry optimization: ethane-3Cl5F, R

0 1
C  0.000000  0.000000  0.000000
C  1.526925 -0.000000  0.000000
Cl -0.397173  1.015461  0.000000
H -0.397164 -0.507733  0.879416
```

```
F -0.397164 -0.507733 -0.879416
H  1.924095 -1.015462 -0.000000
H  1.924090  0.507731 -0.879417
H  1.924090  0.507731  0.879417

ethane_3Cl5F_R_opt.wfx
```

- Dihedral angle scan of optimized structure with steps of +1.0 degrees

```
%NoSave
%NProcShared=4
%Mem=4GB
%chk=ethane_3Cl5F_R_3126_angleplus.chk
#P B3LYP/cc-pVQZ Opt(Modredundant,MaxCycles=999,VeryTight)
scf=(xqc,conver=10,maxcycle=999) Int(Ultrafine) NoSymm

Dihedral scan 3-1-2-6 step +1.0

0 1
C  0.000000  0.000000  0.000000
C  1.504368  0.000000  0.000000
Cl -0.658804  1.682707 -0.000000
H -0.436898 -0.482146  0.870102
F -0.472038 -0.644761 -1.115419
H  1.858996 -1.030715 -0.011734
H  1.880217  0.516783 -0.880358
H  1.881709  0.494668  0.891988

X 1 F
D 3 1 2 6 S 180 1.0
```

Doubly-substituted ethane - Cl,F geometric stereoisomer = 'S'

- Optimization

```
%NoSave
%NProcShared=4
%Mem=4GB
%chk=ethane_3Cl4F_S_start.chk
#P B3LYP/cc-pVQZ Opt(MaxCycles=999,VeryTight) scf=(xqc,conver=10,maxcycle=999)
Int(Ultrafine) NoSymm Output=wfx

Geometry optimization: ethane-3Cl4F, S

0 1
C  0.000000  0.000000  0.000000
C  1.526925 -0.000000  0.000000
Cl -0.397173  1.015461  0.000000
F -0.397164 -0.507733  0.879416
H -0.397164 -0.507733 -0.879416
H  1.924095 -1.015462 -0.000000
H  1.924090  0.507731 -0.879417
H  1.924090  0.507731  0.879417

ethane_3Cl4F_S_opt.wfx
```

- Dihedral angle scan of optimized structure with steps of +1.0 degrees

```
%NoSave
```

```
%NProcShared=4
%Mem=4GB
%chk=ethane_3Cl4F_S_3126_angleplus.chk
#P B3LYP/cc-pVQZ Opt(Modredundant,MaxCycles=999,VeryTight)
scf=(xqc,conver=10,maxcycle=999) Int(Ultrafine) NoSymm

Dihedral scan 3-1-2-6 step +1.0

0 1
C  0.000000  0.000000  0.000000
C  1.504368 -0.000000 -0.000000
Cl -0.658804  1.682707  0.000000
F -0.472038 -0.644761  1.115419
H -0.436898 -0.482146 -0.870102
H  1.858996 -1.030715  0.011734
H  1.881709  0.494668 -0.891988
H  1.880217  0.516783  0.880358

X 1 F
D 3 1 2 6 S 180 1.0
```

Doubly-substituted ethane - Br,Cl, geometric stereoisomer = 'R'

- Optimization

```
%NoSave
%NProcShared=4
%Mem=4GB
%chk=ethane_3Br5Cl_R_start.chk
#P B3LYP/cc-pVQZ Opt(MaxCycles=999,VeryTight) scf=(xqc,conver=10,maxcycle=999)
Int(Ultrafine) NoSymm Output=wfx

Geometry optimization: ethane-3Br5Cl, R

0 1
C  0.000000  0.000000  0.000000
C  1.526925 -0.000000  0.000000
Br -0.397173  1.015461  0.000000
H -0.397164 -0.507733  0.879416
Cl -0.397164 -0.507733 -0.879416
H  1.924095 -1.015462 -0.000000
H  1.924090  0.507731 -0.879417
H  1.924090  0.507731  0.879417

ethane_3Br5Cl_R_opt.wfx
```

- Dihedral angle scan of optimized structure with steps of +1.0 degrees

```
%NoSave
%NProcShared=4
%Mem=4GB
%chk=ethane_3Br5Cl_R_3126_angleplus.chk
#P B3LYP/cc-pVQZ Opt(Modredundant,MaxCycles=999,VeryTight)
scf=(xqc,conver=10,maxcycle=999) Int(Ultrafine) NoSymm

Dihedral scan 3-1-2-6 step +1.0

0 1
C  0.000000  0.000000  0.000000
```

```
C  1.508517 -0.000000  0.000000
Br -0.703935  1.844011  0.000000
H -0.425645 -0.449826  0.886805
Cl -0.652517 -0.922827 -1.391972
H  1.870007 -1.027592  0.038226
H  1.896750  0.475018 -0.897768
H  1.877431  0.537793  0.871890

X 1 F
D 3 1 2 6 S 180 1.0
```

Doubly-substituted ethane - Br,Cl, geometric stereoisomer = 'S'

- Optimization

```
%NoSave
%NProcShared=4
%Mem=4GB
%chk=ethane_3Br4Cl_S_start.chk
#P B3LYP/cc-pVQZ Opt(MaxCycles=999,VeryTight) scf=(xqc,conver=10,maxcycle=999)
Int(Ultrafine) NoSymm Output=wfx

Geometry optimization: ethane-3Br4Cl, S

0 1
C  0.000000  0.000000  0.000000
C  1.526925 -0.000000  0.000000
Br -0.397173  1.015461  0.000000
Cl -0.397164 -0.507733  0.879416
H -0.397164 -0.507733 -0.879416
H  1.924095 -1.015462 -0.000000
H  1.924090  0.507731 -0.879417
H  1.924090  0.507731  0.879417

ethane_3Br4Cl_S_opt.wfx
```

- Dihedral angle scan of optimized structure with steps of +1.0 degrees

```
%NoSave
%NProcShared=4
%Mem=4GB
%chk=ethane_3Br4Cl_S_3126_angleplus.chk
#P B3LYP/cc-pVQZ Opt(Modredundant,MaxCycles=999,VeryTight)
scf=(xqc,conver=10,maxcycle=999) Int(Ultrafine) NoSymm

Dihedral scan 3-1-2-6 step +1.0

0 1
C  0.000000  0.000000  0.000000
C  1.508517 -0.000000  0.000000
Br -0.703935  1.844011  0.000000
Cl -0.652517 -0.922827  1.391972
H -0.425645 -0.449826 -0.886805
H  1.870007 -1.027592 -0.038226
H  1.877431  0.537793 -0.871890
H  1.896750  0.475018  0.897768

X 1 F
D 3 1 2 6 S 180 1.0
```

Doubly-substituted ethane - Br,F, geometric stereoisomer = 'R'

- Optimization

```
%NoSave
%NProcShared=4
%Mem=4GB
%chk=ethane_3Br5F_R_start.chk
#P B3LYP/cc-pVQZ Opt(MaxCycles=999,VeryTight) scf=(xqc,conver=10,maxcycle=999)
Int(Ultrafine) NoSymm Output=wfx

Geometry optimization: ethane-3Br5F, R

0 1
C  0.000000  0.000000  0.000000
C  1.526925 -0.000000  0.000000
Br -0.397173  1.015461  0.000000
H -0.397164 -0.507733  0.879416
F -0.397164 -0.507733 -0.879416
H  1.924095 -1.015462 -0.000000
H  1.924090  0.507731 -0.879417
H  1.924090  0.507731  0.879417

ethane_3Br5F_R_opt.wfx
```

- Dihedral angle scan of optimized structure with steps of +1.0 degrees

```
%NoSave
%NProcShared=4
%Mem=4GB
%chk=ethane_3Br5F_R_3126_angleplus.chk
#P B3LYP/cc-pVQZ Opt(Modredundant,MaxCycles=999,VeryTight)
scf=(xqc,conver=10,maxcycle=999) Int(Ultrafine) NoSymm

Dihedral scan 3-1-2-6 step +1.0

0 1
C  0.000000  0.000000  0.000000
C  1.503013 -0.000000  0.000000
Br -0.722672  1.844686  0.000000
H -0.443216 -0.461973  0.876638
F -0.477711 -0.646195 -1.108534
H  1.854037 -1.033005 -0.006840
H  1.884641  0.509857 -0.881727
H  1.882134  0.496237  0.890157

X 1 F
D 3 1 2 6 S 180 1.0
```

Doubly-substituted ethane - Br,F, geometric stereoisomer = 'S'

- Optimization

```
%NoSave
%NProcShared=4
%Mem=4GB
%chk=ethane_3Br4F_S_start.chk
```

```
#P B3LYP/cc-pVQZ Opt(MaxCycles=999,VeryTight) scf=(xqc,conver=10,maxcycle=999)
Int(Ultrafine) NoSymm Output=wfx

Geometry optimization: ethane-3Br4F, S

0 1
C  0.000000  0.000000  0.000000
C  1.526925 -0.000000  0.000000
Br -0.397173  1.015461  0.000000
F -0.397164 -0.507733  0.879416
H -0.397164 -0.507733 -0.879416
H  1.924095 -1.015462 -0.000000
H  1.924090  0.507731 -0.879417
H  1.924090  0.507731  0.879417

ethane_3Br4F_S_opt.wfx
```

- Dihedral angle scan of optimized structure with steps of +1.0 degrees

```
%NoSave
%NProcShared=4
%Mem=4GB
%chk=ethane_3Br4F_S_3126_angleplus.chk
#P B3LYP/cc-pVQZ Opt(Modredundant,MaxCycles=999,VeryTight)
scf=(xqc,conver=10,maxcycle=999) Int(Ultrafine) NoSymm

Dihedral scan 3-1-2-6 step +1.0

0 1
C  0.000000  0.000000  0.000000
C  1.503013  0.000000  0.000000
Br -0.722672  1.844686  0.000000
F -0.477711 -0.646195  1.108534
H -0.443216 -0.461973 -0.876638
H  1.854037 -1.033005  0.006840
H  1.882134  0.496237 -0.890157
H  1.884641  0.509857  0.881727

X 1 F
D 3 1 2 6 S 180 1.0
```

The dependency of NG-QTAIM quantities on atomic weight of halogen substituents is evident in singly substituted ethane (x = F, Cl, Br), see **Table S5(c)** and doubly substituted ethane, see **Table 5(e)**.

Table S5(a). The maximum stress tensor projections $\{t_{1max}, t_{2max}, t_{3max}\}$ where $\{t_{1max}$ = bond-twist$_{max}$, t_{2max} = bond-flexing$_{max}$, t_{3max} = bond-axiality$_{max}\}$ of the torsion C1-C2 *BCP* of the singly substituted ethane; all entries have been multiplied by 10^3.

$\{t_{1max}$ = bond-twist$_{max}$, t_{2max} = bond-flexing$_{max}$, t_{3max} =bond-axiality$_{max}\}$

Isomer	**CW**	**CCW**
F-ethane		
D_{3126}	{1.555693 , 0.629971 , 0.884194}	{1.555679 , 0.629969 , 0.884172}
D_{3127}	{0.737640 , 1.427344 , 0.882818}	{0.904859 , 1.133955 , 0.888359}
D_{3128}	{0.904748 , 1.133964 , 0.888371}	{0.737578 , 1.426443 , 0.882808}
D_{4126}	{1.484649 , 0.704786 , 0.888406}	{1.492348 , 0.685042 , 0.892077}
D_{4127}	{0.711736 , 1.403303 , 0.890260}	{0.947178 , 1.111342 , 0.889211}
D_{4128}	{0.960596 , 1.129915 , 0.895097}	{0.756835 , 1.367468 , 0.886161}
D_{5126}	{1.492348 , 0.685045 , 0.892077}	{1.484656 , 0.704778 , 0.888395}
D_{5127}	{0.756831 , 1.368459 , 0.886154}	{0.960565 , 1.129775 , 0.895112}
D_{5128}	{0.947216 , 1.111332 , 0.889211}	{0.711746 , 1.402495 , 0.890263}
Cl-ethane		
D_{3126}	{1.357059 , 0.730872 , 0.916115}	{1.357058 , 0.730862 , 0.916121}
D_{3127}	{0.551381 , 1.290424 , 0.914331}	{1.081745 , 1.137342 , 0.899227}
D_{3128}	{1.081850 , 1.137452 , 0.899239}	{0.551448 , 1.290425 , 0.914323}
D_{4126}	{1.402421 , 0.791704 , 0.925166}	{1.344049 , 0.678860 , 0.926557}
D_{4127}	{0.630058 , 1.300000 , 0.925025}	{1.155498 , 1.143646 , 0.905805}
D_{4128}	{0.983929 , 1.210597 , 0.908156}	{0.571040 , 1.339648 , 0.922197}
D_{5126}	{1.344042 , 0.678863 , 0.926558}	{1.402430 , 0.791742 , 0.925166}
D_{5127}	{0.571009 , 1.339349 , 0.922203}	{0.985005 , 1.211563 , 0.908164}
D_{5128}	{1.155544 , 1.143652 , 0.905798}	{0.630057 , 1.300008 , 0.925029}
Br-ethane		
D_{3126}	{1.328622, 0.767338, 0.902567}	{1.328574, 0.767351, 0.902554}
D_{3127}	{0.538959, 1.298727, 0.901220}	{1.122824, 1.138762, 0.876074}
D_{3128}	{1.122951, 1.138761, 0.876061}	{0.538966, 1.298822, 0.901232}
D_{4126}	{1.422407, 0.813149, 0.912225}	{1.343162, 0.658898, 0.913455}
D_{4127}	{0.665783, 1.315357, 0.911682}	{1.206685, 1.148845, 0.883079}
D_{4128}	{0.962986, 1.231180, 0.883283}	{0.575332, 1.393254, 0.910309}
D_{5126}	{1.343125, 0.658826, 0.913456}	{1.422440, 0.813230, 0.912229}
D_{5127}	{0.575384, 1.393371, 0.910289}	{0.963061, 1.230208, 0.883273}
D_{5128}	{1.206701, 1.148971, 0.883102}	{0.665921, 1.315400, 0.911683}

Table S5(b). The complete C1-C2 *BCP* U_σ-space distortion sets for singly substituted ethane. The sum of the nine isomers: $\sum_{S\sigma,R\sigma}\{C_\sigma,F_\sigma,B_\sigma\}$, sum of the S_σ components $\sum_{S\sigma}\{C_\sigma,B_\sigma\}$ and R_σ components $\sum_{R\sigma}\{C_\sigma,B_\sigma\}$, chirality-helicity function $C_{helicity} = (C_\sigma)(|B_\sigma|)$ and the sum of $C_{helicity}$ over the nine isomers $\sum C_{helicity}$. The classification $[C_\sigma,B_\sigma]$ is Q_σ when the $\sum C_{helicity} = 0$.

F-ethane

Isomer	$\{C_\sigma, F_\sigma, B_\sigma\}$	$C_{helicity}$	$[C_\sigma,B_\sigma]$
D_{3126}	{-0.000014**[R_σ]**, -0.000002**[R_σ]**, -0.000022**[R_σ]**}	0 (-3.14×10^{-10})	**[Q_σ]**
D_{3127}	{0.167219**[S_σ]**, -0.293389**[R_σ]**, 0.005542**[S_σ]**}	0.0009	**[S_σ,S_σ]**
D_{3128}	{-0.167170**[R_σ]**, 0.292479**[S_σ]**, -0.005563**[R_σ]**}	-0.0009	**[R_σ,R_σ]**
D_{4126}	{0.007700**[S_σ]**, -0.019744**[R_σ]**, 0.003671**[S_σ]**}	0 (2.83×10^{-5})	**[Q_σ]**
D_{4127}	{0.235443**[S_σ]**, -0.291961**[R_σ]**, -0.001050**[R_σ]**}	0.0002	**[S_σ,R_σ]**
D_{4128}	{-0.203761**[R_σ]**, 0.237553**[S_σ]**, -0.008936**[R_σ]**}	-0.0018	**[R_σ,R_σ]**
D_{5126}	{-0.007692**[R_σ]**, 0.019733**[S_σ]**, -0.003683**[R_σ]**}	0 (-2.83×10^{-5})	**[Q_σ]**
D_{5127}	{0.203734**[S_σ]**, -0.238685**[R_σ]**, 0.008958**[S_σ]**}	0.0018	**[S_σ,S_σ]**
D_{5128}	{-0.235470**[R_σ]**, 0.291163**[S_σ]**, 0.001052**[S_σ]**}	-0.0002	**[R_σ,S_σ]**

Sum of the S_σ subset from all nine isomers	*Sum of the R_σ subset from all nine isomers*
$\sum_{S\sigma}\{C_\sigma,B_\sigma\}$	$\sum_{R\sigma}\{C_\sigma,B_\sigma\}$
{0.6141**[S_σ]**, 0.0192**[S_σ]**}	{-0.6141**[R_σ]**, -0.0193**[R_σ]**}

Total sum of all nine isomers

$\sum_{S\sigma,R\sigma}\{C_\sigma, F_\sigma, B_\sigma\}$	$\sum C_{helicity}$	
{-0.00001**[R_σ]**, -0.0029**[R_σ]**, -0.00003**[R_σ]**}	0	**[Q_σ]**

Cl-ethane

Isomer	$\{C_\sigma, F_\sigma, B_\sigma\}$	$C_{helicity}$	$[C_\sigma,B_\sigma]$
D_{3126}	{-0.000001**[R_σ]**, -0.000009**[R_σ]**, 0.000006**[S_σ]**}	0 (-7.65×10^{-12})	**[Q_σ]**
D_{3127}	{0.530364**[S_σ]**, -0.153082**[R_σ]**, -0.015103**[R_σ]**}	0.0080	**[S_σ,R_σ]**
D_{3128}	{-0.530402**[R_σ]**, 0.152974**[S_σ]**, 0.015084**[S_σ]**}	-0.0080	**[R_σ,S_σ]**
D_{4126}	{-0.058372**[R_σ]**, -0.112844**[R_σ]**, 0.001391**[S_σ]**}	0 (-8.12×10^{-5})	**[Q_σ]**
D_{4127}	{0.525440**[S_σ]**, -0.156354**[R_σ]**, -0.019219**[R_σ]**}	0.0101	**[S_σ,R_σ]**
D_{4128}	{-0.412889**[R_σ]**, 0.129050**[S_σ]**, 0.014041**[S_σ]**}	-0.0058	**[R_σ,S_σ]**
D_{5126}	{0.058388**[S_σ]**, 0.112880**[S_σ]**, -0.001392**[R_σ]**}	0 (-8.13×10^{-5})	**[Q_σ]**
D_{5127}	{0.413996**[S_σ]**, -0.127786**[R_σ]**, -0.014039**[R_σ]**}	0.0058	**[S_σ,R_σ]**
D_{5128}	{-0.525488**[R_σ]**, 0.156356**[S_σ]**, 0.019231**[S_σ]**}	-0.0101	**[R_σ,S_σ]**

Sum of the S_σ subset from all nine isomers	*Sum of the R_σ subset from all nine isomers*
$\sum_{S\sigma}\{C_\sigma,B_\sigma\}$	$\sum_{R\sigma}\{C_\sigma,B_\sigma\}$
{1.5282**[S_σ]**, 0.0498**[S_σ]**}	{-1.5272**[R_σ]**, -0.0498**[R_σ]**}

Total sum of all nine isomers

$\sum_{S\sigma,R\sigma}\{C_\sigma, F_\sigma, B_\sigma\}$	$\sum C_{helicity}$	
{0.0010**[S_σ]**, 0.0012**[S_σ]**, 0.000006**[S_σ]**}	0	**[Q_σ]**

Br-ethane

Isomer	$\{C_\sigma, F_\sigma, B_\sigma\}$	$C_{helicity}$	$[C_\sigma,B_\sigma]$
D_{3126}	{-0.000049**[R_σ]**, 0.000013**[S_σ]**, -0.000012**[R_σ]**}	0 (-5.84×10^{-10})	**[Q_σ]**
D_{3127}	{0.583865**[S_σ]**, -0.159965**[R_σ]**, -0.025146**[R_σ]**}	0.0147	**[S_σ,R_σ]**
D_{3128}	{-0.583985**[R_σ]**, 0.160061**[S_σ]**, 0.025172**[S_σ]**}	-0.0147	**[R_σ,S_σ]**
D_{4126}	{-0.079245**[R_σ]**, -0.154251**[R_σ]**, 0.001230**[S_σ]**}	0 (-9.74×10^{-5})	**[Q_σ]**
D_{4127}	{0.540902**[S_σ]**, -0.166512**[R_σ]**, -0.028603**[R_σ]**}	0.0155	**[S_σ,R_σ]**
D_{4128}	{-0.387654**[R_σ]**, 0.162074**[S_σ]**, 0.027027**[S_σ]**}	-0.0105	**[R_σ,S_σ]**
D_{5126}	{0.079315**[S_σ]**, 0.154404**[S_σ]**, -0.001227**[R_σ]**}	0 (-9.73×10^{-5})	**[Q_σ]**
D_{5127}	{0.387677**[S_σ]**, -0.163163**[R_σ]**, -0.027016**[R_σ]**}	0.0105	**[S_σ,R_σ]**
D_{5128}	{-0.540781**[R_σ]**, 0.166429**[S_σ]**, 0.028581**[S_σ]**}	-0.0155	**[R_σ,S_σ]**

Sum of the S_σ subset from all nine isomers	*Sum of the R_σ subset from all nine isomers*

$\sum_{S\sigma}\{C_\sigma,B_\sigma\}$	$\sum_{R\sigma}\{C_\sigma,B_\sigma\}$	
{1.5918**[S_σ]**, 0.0820**[S_σ]**}	{-1.5917**[R_σ]**, -0.0820**[R_σ]**}	
Total sum of all nine isomers		
$\sum_{S\sigma,R\sigma}\{C_\sigma,F_\sigma,B_\sigma\}$	$\sum C_{helicity}$	
{0.00005**[S_σ]**, -0.0009**[R_σ]**, 0.000006**[S_σ]**}	0	**[Q_σ]**

Table S5(c). The singly substituted ethane torsion C1-C2 *BCP* U_σ-space distortion sets sum of the nine isomers: $\sum\{C_\sigma, F_\sigma, B_\sigma\}$, the chirality-helicity function $C_{helicity}$ and the sum over the nine isomers $\sum C_{helicity}$. The values of the total sums in the table correspond to all nine isomers, see **Figure 3** (Top).

	$\sum\{C_\sigma,F_\sigma,B_\sigma\}$	$\sum C_{helicity}$	$[C_\sigma,B_\sigma]$
F-ethane	{-0.00001[$\mathbf{R}_\sigma$]}, -0.0029[$\mathbf{R}_\sigma$], -0.00003[$\mathbf{R}_\sigma$]	0	$\mathbf{Q}_\sigma$
Cl-ethane	{0.0010[$\mathbf{S}_\sigma$]}, 0.0012 [$\mathbf{S}_\sigma$], 0.000006[$\mathbf{S}_\sigma$]}	0	$\mathbf{Q}_\sigma$
Br-ethane	{0.00005[$\mathbf{S}_\sigma$]}, -0.0009[$\mathbf{R}_\sigma$], 0.000006[$\mathbf{S}_\sigma$]}	0	$\mathbf{Q}_\sigma$

Table S5(d). The maximum stress tensor projections $\{\boldsymbol{t}_{1max}, \boldsymbol{t}_{2\ max}, \boldsymbol{t}_{3max}\}$ where $\{\boldsymbol{t}_{1max}$ = bond-twist$_{max}$, $\boldsymbol{t}_{2max}$ = bond-flexing$_{max}$, $\boldsymbol{t}_{3max}$ = bond-axiality$_{max}\}$of the torsion C1-C2 *BCP* of the doubly substituted ethane; all entries have been multiplied by 10^3.

$\{\boldsymbol{t}_{1max}$ = bond-twist$_{max}$, $\boldsymbol{t}_{2max}$ = bond-flexing$_{max}$, $\boldsymbol{t}_{3max}$ =bond-axiality$_{max}\}$

	S		*R*	
Isomer	CW	CCW	CW	CCW
F-Cl-ethane				
D_{3126}	{0.846468, 0.976609, 0.942658}	{0.988526, 1.075026, 0.966650}	{0.988444, 1.075045, 0.966644}	{0.846326, 0.975950,0.942661}
D_{3127}	{0.659022, 0.905559, 0.969447}	{1.203876, 0.976404, 0.936509}	{0.935701, 0.581193, 0.952897}	{1.259820, 1.165087, 0.922876}
D_{3128}	{1.259063, 1.165104, 0.922892}	{0.935785, 0.580947, 0.952866}	{1.204035, 0.976337, 0.936472}	{0.659022, 0.905549, 0.969447}
D_{4126}	{0.803155, 0.982214, 0.939244}	{0.943215, 1.091686, 0.966443}	{0.886856, 1.191857, 0.976194}	{0.767363, 0.967764, 0.947866}
D_{4127}	{0.722888, 0.830620, 0.970062}	{1.254937, 0.925794, 0.937573}	{0.986334, 0.558148, 0.959599}	{1.348381, 1.132872, 0.935636}
D_{4128}	{1.218252, 1.194782, 0.924424}	{0.906080, 0.594123, 0.951198}	{1.189047, 0.894842, 0.943250}	{0.769064, 0.923840, 0.979118}
D_{5126}	{0.767334, 0.968046, 0.947872}	{0.886771, 1.191813, 0.975703}	{0.943287, 1.091658, 0.966439}	{0.803068, 0.982226, 0.939257}
D_{5127}	{0.769023, 0.924002, 0.979118}	{1.189011, 0.894853, 0.943281}	{0.906204, 0.594014, 0.951189}	{1.218391, 1.194672, 0.924423}
D_{5128}	{1.348409, 1.132696, 0.935643}	{0.986185, 0.558013, 0.959610}	{1.254977, 0.925679, 0.937573}	{0.722888, 0.830622, 0.970067}
Cl-Br-ethane				
D_{3126}	{1.173687, 1.197140, 1.032246}	{1.316034, 1.070201, 1.062299}	{1.316150, 1.070154, 1.062290}	{1.173744, 1.195733, 1.032257}
D_{3127}	{0.634147, 0.789749, 1.077466}	{1.445078, 1.127301, 1.023793}	{1.168076, 0.798776, 1.033466}	{1.251175, 1.139944, 1.029045}
D_{3128}	{1.251951, 1.140018, 1.029056}	{1.168312, 0.798701, 1.033469}	{1.445121, 1.128060, 1.023714}	{0.634145, 0.789661, 1.077454}
D_{4126}	{1.244701, 1.065434, 1.025801}	{1.329705, 1.023315, 1.060648}	{1.112841, 1.375915, 1.085900}	{1.050902, 1.067195, 1.043821}
D_{4127}	{0.578879, 0.800453, 1.075229}	{1.383568, 1.211384, 1.024576}	{1.451627, 0.535171, 1.053942}	{1.565837, 0.851010, 1.049937}
D_{4128}	{1.187683, 1.077432, 1.029527}	{1.224909, 0.855543, 1.032604}	{1.249372, 1.011148, 1.033814}	{0.777781, 1.086836, 1.098234}
D_{5126}	{1.050887, 1.067184, 1.043820}	{1.112743, 1.375933, 1.085892}	{1.329823, 1.023480, 1.060645}	{1.244513, 1.065295, 1.025809}
D_{5127}	{0.777780, 1.086897, 1.098237}	{1.249194, 1.012180, 1.033796}	{1.225044, 0.855567, 1.032606}	{1.187148, 1.077417, 1.029532}
D_{5128}	{1.565169, 0.850982, 1.050045}	{1.451476, 0.535173, 1.053936}	{1.383406, 1.210706, 1.024552}	{0.578890, 0.800518, 1.075234}
Br-F-ethane				

D_{3126}	{0.850025, 1.054332, 0.947375}	{1.036695, 1.088110, 0.971936}	{1.036705, 1.088203, 0.971940}	{0.850142, 1.054357, 0.947379}
D_{3127}	{0.768754, 0.861907, 0.976164}	{1.231786, 1.021431, 0.932925}	{0.972755, 0.548857, 0.950086}	{1.245720, 1.261749, 0.919209}
D_{3128}	{1.245787, 1.261718, 0.919241}	{0.972753, 0.548856, 0.950083}	{1.231839, 1.022144, 0.932931}	{0.768750, 0.861956, 0.976159}
D_{4126}	{0.854249, 1.031163, 0.943642}	{1.009021, 1.076311, 0.970898}	{0.918303, 1.237360, 0.983423}	{0.749535, 1.028341, 0.953244}
D_{4127}	{0.803565, 0.812166, 0.975615}	{1.249512, 0.999977, 0.933360}	{1.039124, 0.542685, 0.958047}	{1.367632, 1.195804, 0.932595}
D_{4128}	{1.181085, 1.271019, 0.919907}	{0.957800, 0.596778, 0.948890}	{1.188886, 0.906254, 0.938593}	{0.909459, 0.956267, 0.987097}
D_{5126}	{0.749559, 1.027674, 0.953234}	{0.918212, 1.237194, 0.983416}	{1.009081, 1.076479, 0.970893}	{0.854343, 1.031150, 0.943681}
D_{5127}	{0.909441, 0.956239, 0.987121}	{1.188755, 0.907182, 0.938601}	{0.957713, 0.596859, 0.948884}	{1.181733, 1.271109, 0.919894}
D_{5128}	{1.368486, 1.195732, 0.932657}	{1.039223, 0.542627, 0.958016}	{1.249317, 0.999865, 0.933438}	{0.803550, 0.812194, 0.975592}

Table S5(e). Doubly substituted ethane torsion C1-C2 *BCP* U_{σ}-space distortion sets $\{C_{\sigma},F_{\sigma},B_{\sigma}\}$.

F-Cl-ethane

S_a				R_a			
Isomer	$\{C_{\sigma}, F_{\sigma}, B_{\sigma}\}$	$C_{helicity}$	$[C_{\sigma},B_{\sigma}]$	$\{C_{\sigma}, F_{\sigma}, B_{\sigma}\}$	$C_{helicity}$	$[C_{\sigma},B_{\sigma}]$	
D_{3126}	{0.142058**[S_{σ}]**, 0.098417**[S_{σ}]**, 0.023993**[S_{σ}]**}	0.0034	**[S_{σ},S_{σ}]**	{-0.142118**[R_{σ}]**, -0.099095**[R_{σ}]**, -0.023983**[R_{σ}]**}	-0.0034	**[R_{σ},R_{σ}]**	
D_{3127}	{0.544855**[S_{σ}]**, 0.070844**[S_{σ}]**, -0.032938**[R_{σ}]**}	0.0179	**[S_{σ},R_{σ}]**	{0.324119**[S_{σ}]**, 0.583893**[S_{σ}]**, -0.030021**[R_{σ}]**}	0.0097	**[S_{σ},R_{σ}]**	
D_{3128}	{-0.323278**[R_{σ}]**, -0.584156**[R_{σ}]**, 0.029974**[S_{σ}]**}	-0.0097	**[R_{σ},S_{σ}]**	{-0.545013**[R_{σ}]**, -0.070787**[R_{σ}]**, 0.032975**[S_{σ}]**}	-0.0180	**[R_{σ},S_{σ}]**	
D_{4126}	{0.140060**[S_{σ}]**, 0.109472**[S_{σ}]**, 0.027200**[S_{σ}]**}	0.0038	**[S_{σ},S_{σ}]**	{-0.119493**[R_{σ}]**, -0.224093**[R_{σ}]**, -0.028328**[R_{σ}]**}	-0.0034	**[R_{σ},R_{σ}]**	
D_{4127}	{0.532049**[S_{σ}]**, 0.095174**[S_{σ}]**, -0.032489**[R_{σ}]**}	0.0173	**[S_{σ},R_{σ}]**	{0.362047**[S_{σ}]**, 0.574724**[S_{σ}]**, -0.023964**[R_{σ}]**}	0.0087	**[S_{σ},R_{σ}]**	
D_{4128}	{-0.312172**[R_{σ}]**, -0.600659**[R_{σ}]**, 0.026774**[S_{σ}]**}	-0.0084	**[R_{σ},S_{σ}]**	{-0.419983**[R_{σ}]**, 0.028998**[S_{σ}]**, 0.035868**[S_{σ}]**}	-0.0151	**[R_{σ},S_{σ}]**	
D_{5126}	{0.119437**[S_{σ}]**, 0.223768**[S_{σ}]**, 0.027831**[S_{σ}]**}	0.0033	**[S_{σ},S_{σ}]**	{-0.140219**[R_{σ}]**, -0.109432**[R_{σ}]**, -0.027182**[R_{σ}]**}	-0.0038	**[R_{σ},R_{σ}]**	
D_{5127}	{0.419988**[S_{σ}]**, -0.029150**[R_{σ}]**, -0.035837**[R_{σ}]**}	0.0151	**[S_{σ},R_{σ}]**	{0.312187**[S_{σ}]**, 0.600659**[S_{σ}]**, -0.026766**[R_{σ}]**}	0.0084	**[S_{σ},R_{σ}]**	
D_{5128}	{-0.362224**[R_{σ}]**, -0.574683**[R_{σ}]**, 0.023966**[S_{σ}]**}	-0.0087	**[R_{σ},S_{σ}]**	{-0.532089**[R_{σ}]**, -0.095057**[R_{σ}]**, 0.032494**[S_{σ}]**}	-0.0173	**[R_{σ},S_{σ}]**	
Total sum of all nine isomers of S_a				*Total sum of all nine isomers of R_a*			
$\sum_{S\sigma,R\sigma}\{C_{\sigma}, F_{\sigma}, B_{\sigma}\}$		$\sum C_{helicity}$		$\sum_{S\sigma,R\sigma}\{C_{\sigma}, F_{\sigma}, B_{\sigma}\}$		$\sum C_{helicity}$	
{0.9008 **[S_{σ}]**, -1.1910 **[R_{σ}]**, 0.0585 **[S_{σ}]**}		0.0340	**[S_{σ},S_{σ}]**	{-0.9006 **[R_{σ}]**, 1.1898 **[S_{σ}]**, -0.0589 **[R_{σ}]**}		-0.0342	**[R_{σ},R_{σ}]**
Sum of the S_{σ}, R_{σ} subsets from all nine S_a isomers				*Sum of the S_{σ}, R_{σ} subsets from all nine R_a isomers*			
$\sum_{S\sigma}\{C_{\sigma},B_{\sigma}\}$	$\sum_{R\sigma}\{C_{\sigma},B_{\sigma}\}$			$\sum_{S\sigma}\{C_{\sigma},B_{\sigma}\}$	$\sum_{R\sigma}\{C_{\sigma},B_{\sigma}\}$		
{1.8984 **[S_{σ}]**, 0.1597 **[S_{σ}]**}	{-0.9977 **[R_{σ}]**, -0.1013 **[R_{σ}]**}			{0.9984 **[S_{σ}]**, 0.1013 **[S_{σ}]**}	{-1.8989 **[R_{σ}]**, -0.1602 **[R_{σ}]**}		
Ratio of the S_{σ} and R_{σ} subsets from all nine S_a isomers							
$\sum_{S\sigma}\{C_{\sigma}\}/\lvert\sum_{R\sigma}\{C_{\sigma}\}\rvert\}$ $\lvert S_a$ = **1.903**							

Cl-Br-ethane

Isomer	$\{C_{\sigma}, F_{\sigma}, B_{\sigma}\}$	$C_{helicity}$	$[C_{\sigma},B_{\sigma}]$	$\{C_{\sigma}, F_{\sigma}, B_{\sigma}\}$	$C_{helicity}$	$[C_{\sigma},B_{\sigma}]$	
D_{3126}	{0.142347**[S_{σ}]**, -0.126939**[R_{σ}]**, 0.030052**[S_{σ}]**}	0.0043	**[S_{σ},S_{σ}]**	{-0.142405**[R_{σ}]**, 0.125579**[S_{σ}]**, -0.030034**[R_{σ}]**}	-0.0043	**[R_{σ},R_{σ}]**	
D_{3127}	{0.810931**[S_{σ}]**, 0.337552**[S_{σ}]**, -0.053673**[R_{σ}]**}	0.0435	**[S_{σ},R_{σ}]**	{0.083099**[S_{σ}]**, 0.341168**[S_{σ}]**, -0.004421**[R_{σ}]**}	0.0004	**[S_{σ},R_{σ}]**	
D_{3128}	{-0.083639**[R_{σ}]**, -0.341316**[R_{σ}]**, 0.004413**[S_{σ}]**}	-0.0004	**[R_{σ},S_{σ}]**	{-0.810976**[R_{σ}]**, -0.338399**[R_{σ}]**, 0.053740**[S_{σ}]**}	-0.0436	**[R_{σ},S_{σ}]**	
D_{4126}	{0.085004**[S_{σ}]**, -0.042120**[R_{σ}]**, 0.034848**[S_{σ}]**}	0.0030	**[S_{σ},S_{σ}]**	{-0.061939**[R_{σ}]**, -0.308720**[R_{σ}]**, -0.042080**[R_{σ}]**}	-0.0026	**[R_{σ},R_{σ}]**	
D_{4127}	{0.804689**[S_{σ}]**, 0.410931**[S_{σ}]**, -0.050652**[R_{σ}]**}	0.0408	**[S_{σ},R_{σ}]**	{0.114210**[S_{σ}]**, 0.315839**[S_{σ}]**, -0.004005**[R_{σ}]**}	0.0005	**[S_{σ},R_{σ}]**	
D_{4128}	{0.037226**[S_{σ}]**, -0.221889**[R_{σ}]**, 0.003077**[S_{σ}]**}	0.0001	**[S_{σ},S_{σ}]**	{-0.471592**[R_{σ}]**, 0.075689**[S_{σ}]**, 0.064420**[S_{σ}]**}	-0.0304	**[R_{σ},S_{σ}]**	
D_{5126}	{0.061856**[S_{σ}]**, 0.308749**[S_{σ}]**, 0.042072**[S_{σ}]**}	0.0026	**[S_{σ},S_{σ}]**	{-0.085311**[R_{σ}]**, 0.041815**[S_{σ}]**, -0.034836**[R_{σ}]**}	-0.0030	**[R_{σ},R_{σ}]**	
D_{5127}	{0.471413**[S_{σ}]**, -0.074717**[R_{σ}]**, -0.064441**[R_{σ}]**}	0.0304	**[S_{σ},R_{σ}]**	{-0.037897**[R_{σ}]**, 0.221850**[S_{σ}]**, -0.003074**[R_{σ}]**}	-0.0001	**[R_{σ},R_{σ}]**	
D_{5128}	{-0.113693**[R_{σ}]**, -0.315810**[R_{σ}]**, 0.003891**[S_{σ}]**}	-0.0004	**[R_{σ},S_{σ}]**	{-0.804516**[R_{σ}]**, -0.410188**[R_{σ}]**, 0.050681**[S_{σ}]**}	-0.0408	**[R_{σ},S_{σ}]**	
Total sum of all nine isomers of S_a				*Total sum of all nine isomers of R_a*			
$\sum_{S\sigma,R\sigma}\{C_{\sigma}, F_{\sigma}, B_{\sigma}\}$		$\sum C_{helicity}$		$\sum_{S\sigma,R\sigma}\{C_{\sigma}, F_{\sigma}, B_{\sigma}\}$		$\sum C_{helicity}$	
{2.2161 **[S_{σ}]**, -0.0656 **[R_{σ}]**, -0.0504 **[R_{σ}]**}		0.1239	**[S_{σ},R_{σ}]**	{-2.2173 **[R_{σ}]**, 0.0646 **[S_{σ}]**, 0.0504 **[S_{σ}]**}		-0.1239	**[R_{σ},S_{σ}]**
Sum of the S_{σ}, R_{σ} subsets from all nine S_a isomers				*Sum of the S_{σ}, R_{σ} subsets from all nine R_a isomers*			
$\sum_{S\sigma}\{C_{\sigma},B_{\sigma}\}$	$\sum_{R\sigma}\{C_{\sigma},B_{\sigma}\}$			$\sum_{S\sigma}\{C_{\sigma},B_{\sigma}\}$	$\sum_{R\sigma}\{C_{\sigma},B_{\sigma}\}$		
{2.4135 **[S_{σ}]**, 0.1184 **[S_{σ}]**}	{-0.1973 **[R_{σ}]**, -0.1688 **[R_{σ}]**}			{0.1973 **[S_{σ}]**, 0.1688 **[S_{σ}]**}	{-2.4146 **[R_{σ}]**, -0.1185 **[R_{σ}]**}		
Ratio of the S_{σ} and R_{σ} subsets from all nine S_a isomers							
$\sum_{S\sigma}\{C_{\sigma}\}/\lvert\sum_{R\sigma}\{C_{\sigma}\}\rvert\}$ $\lvert S_a$ = **12.233**							

Br-F-ethane

Isomer	$\{C_\sigma, F_\sigma, B_\sigma\}$	$C_{helicity}$	$[C_\sigma,B_\sigma]$	$\{C_\sigma, F_\sigma, B_\sigma\}$	$C_{helicity}$	$[C_\sigma,B_\sigma]$
D_{3126}	{0.186670**[S_σ]**, 0.033778**[S_σ]**, 0.024561**[S_σ]**}	0.0046	**[S_σ,S_σ]**	{-0.186563**[R_σ]**, -0.033845**[R_σ]**, -0.024561**[R_σ]**}	-0.0046	**[R_σ,R_σ]**
D_{3127}	{0.463032**[S_σ]**, 0.159524**[S_σ]**, -0.043239**[R_σ]**}	0.0200	**[S_σ,R_σ]**	{0.272965**[S_σ]**, 0.712893**[S_σ]**, -0.030877**[R_σ]**}	0.0084	**[S_σ,R_σ]**
D_{3128}	{-0.273034**[R_σ]**, -0.712862**[R_σ]**, 0.030841**[S_σ]**}	-0.0084	**[R_σ,S_σ]**	{-0.463089**[R_σ]**, -0.160188**[R_σ]**, 0.043228**[S_σ]**}	-0.0200	**[R_σ,S_σ]**
D_{4126}	{0.154772**[S_σ]**, 0.045147**[S_σ]**, 0.027256**[S_σ]**}	0.0042	**[S_σ,S_σ]**	{-0.168768**[R_σ]**, -0.209019**[R_σ]**, -0.030179**[R_σ]**}	-0.0051	**[R_σ,R_σ]**
D_{4127}	{0.445947**[S_σ]**, 0.187811**[S_σ]**, -0.042255**[R_σ]**}	0.0188	**[S_σ,R_σ]**	{0.328508**[S_σ]**, 0.653119**[S_σ]**, -0.025453**[R_σ]**}	0.0084	**[S_σ,R_σ]**
D_{4128}	{-0.223285**[R_σ]**, -0.674241**[R_σ]**, 0.028982**[S_σ]**}	-0.0065	**[R_σ,S_σ]**	{-0.279427**[R_σ]**, 0.050013**[S_σ]**, 0.048504**[S_σ]**}	-0.0136	**[R_σ,S_σ]**
D_{5126}	{0.168652**[S_σ]**, 0.209520**[S_σ]**, 0.030182**[S_σ]**}	0.0051	**[S_σ,S_σ]**	{-0.154738**[R_σ]**, -0.045329**[R_σ]**, -0.027212**[R_σ]**}	-0.0042	**[R_σ,R_σ]**
D_{5127}	{0.279314**[S_σ]**, -0.049058**[R_σ]**, -0.048520**[R_σ]**}	0.0136	**[S_σ,R_σ]**	{0.224020**[S_σ]**, 0.674250**[S_σ]**, -0.028989**[R_σ]**}	0.0065	**[S_σ,R_σ]**
D_{5128}	{-0.329263**[R_σ]**, -0.653104**[R_σ]**, 0.025360**[S_σ]**}	-0.0083	**[R_σ,S_σ]**	{-0.445767**[R_σ]**, -0.187671**[R_σ]**, 0.042154**[S_σ]**}	-0.0188	**[R_σ,S_σ]**
Total sum of all nine isomers of S_a				*Total sum of all nine isomers of R_a*		
$\sum_{S\sigma,R\sigma}\{C_\sigma, F_\sigma, B_\sigma\}$		$\sum C_{helicity}$		$\sum_{S\sigma,R\sigma}\{C_\sigma, F_\sigma, B_\sigma\}$		$\sum C_{helicity}$
{0.8728 **[S_σ]**, -1.4535 **[R_σ]**, 0.0332 **[S_σ]**}		0.0431	**[S_σ,S_σ]**	{-0.8729 **[R_σ]**, 1.4542 **[S_σ]**, -0.0334 **[R_σ]**}		-0.0430 **[R_σ,R_σ]**
Sum of the S_σ, R_σ subsets from all nine S_a isomers				*Sum of the S_σ, R_σ subsets from all nine R_a isomers*		
$\sum_{S\sigma}\{C_\sigma,B_\sigma\}$	$\sum_{R\sigma}\{C_\sigma,B_\sigma\}$			$\sum_{S\sigma}\{C_\sigma,B_\sigma\}$	$\sum_{R\sigma}\{C_\sigma,B_\sigma\}$	
{1.6984 **[S_σ]**, 0.1672 **[S_σ]**}	{-0.8256 **[R_σ]**, -0.1340 **[R_σ]**}			{0.8255 **[S_σ]**, 0.1339 **[S_σ]**}	{-1.6984 **[R_σ]**, -0.1673 **[R_σ]**}	
Ratio of the S_σ and R_σ subsets from all nine S_a isomers						
$\sum_{S\sigma}\{C_\sigma\}/\lvert\sum_{R\sigma}\{C_\sigma\}\rvert\}$ $\lvert S_a$ = **2.057**						

Consideration of the doubly halogen-substituted ethane molecules demonstrated agreement with the CIP rules, however, also a mix of $\mathbf{S_\sigma}$ and $\mathbf{R_\sigma}$ chirality C_σ assignments for each of the S and R geometric stereoisomers. The greatest $\mathbf{S_\sigma}$ and $\mathbf{R_\sigma}$ mixing was found when one of the substituent atoms was F. Doubly substituted ethane with the lowest mixed chirality in U_σ-space is Cl-Br-ethane, where $\sum_{S\sigma}\{C_\sigma\}/\sum_{R\sigma}\{C_\sigma\} \approx 12$. In contrast, F-Br-ethane and Br-F-ethane both possess $\sum_{S\sigma}\{C_\sigma\}/\sum_{R\sigma}\{C_\sigma\} \approx 2$, see the bold entries in **Table S5(e).** No dependency of the halogen substituent atomic weight on the morphology of the $T_\sigma(s)$ was apparent for the doubly halogen-substituted ethane, see **Figure S5**.

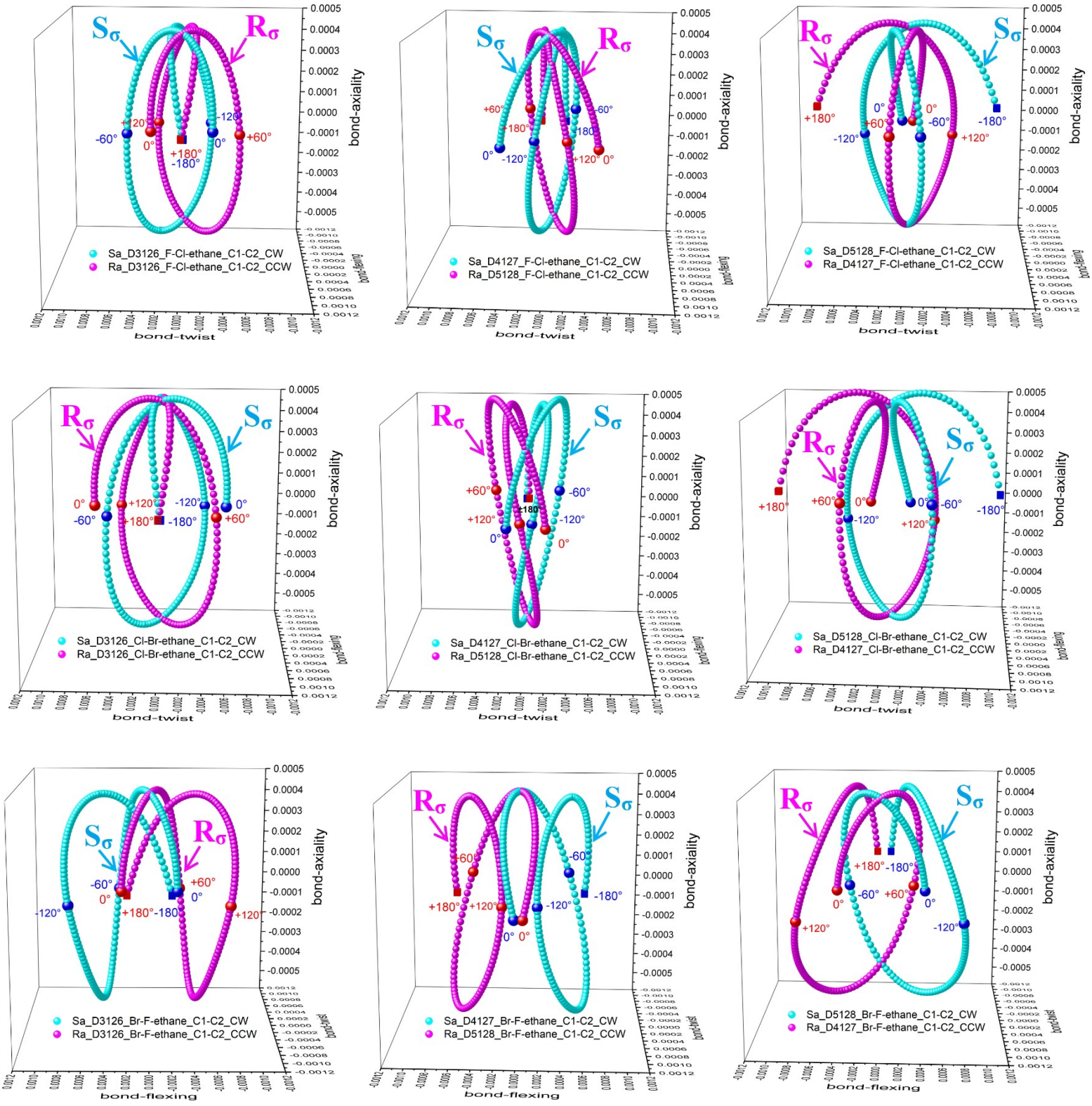

Figure S5. The doubly substituted ethane C1-C2 *BCP* stress tensor trajectories $\mathsf{T}_{\boldsymbol{\sigma}}(s)$ for the Cartesian CW and CCW torsions for S_a and R_a stereoisomers of the $\mathbf{S}_{\boldsymbol{\sigma}}$ and $\mathbf{R}_{\boldsymbol{\sigma}}$ $\mathsf{U}_{\boldsymbol{\sigma}}$-space isomers the F-Cl-ethane, Cl-Br-ethane and Br-F-ethane are provided in the top, middle and bottom panels, see **Table S5(e)**.

6. Supplementary Materials S6. Full Symmetry-Breaking and Relevance for Stereochemistry: Electric field induced mixed S and R chiral character

For the geometry optimizations, the standard alignment was defined as: Atom C3 at the origin, bond C3-C10 along the x-axis and atom C1 defining the x-y plane. Geometry optimizations performed in a non-zero electric field (applied along the x-axis) were done in an iterative manner. At each iteration, the molecule was geometry-optimized with the non-zero field applied along the x-axis, then the result realigned to the standard alignment. Ten iterations of this 'optimize-realign' cycle were found to be sufficient to give negligible changes on successive iterations. This was necessary as it was only possible to specify the electric field direction in terms of the global coordinate system and not as being consistently along a specific bond. Different electronic structure packages have different capabilities in this regard.

Zero-field aligned geometry-optimized structures and Gaussian input files for constrained optimization with dihedral angle scanning are listed below. Only the input files for dihedral angle scanning for the 3-1-2-7 dihedral angle with steps of +1.0 degrees are listed - the corresponding files for scanning with steps of -1.0 degrees and the other possible dihedral angles are omitted for brevity. These are identical except that a) the last number on the last line (beginning with 'D') should be -1.0 rather than 1.0 and b) the atom numbers defining the dihedral, i.e. appearing immediately after the 'D', are modified accordingly. Once field-optimized, the C3-C10 bond distance is constrained to be constant during the dihedral scans and the C1 atom is constrained to be at the origin of coordinates.

Geometry optimized zero-field structure of R-alanine (standard alignment, .xyz format)

```
13
geom opt E=-3.239066694749e+02 R-alanine
C -0.8414389884  1.2944103772  0.0000000000
C -0.2479078576  2.3365078012 -0.9444013242
C  0.0000000000  0.0000000000  0.0000000000
N -2.2552642078  0.9681443636 -0.2492518980
H -0.7691780590  1.6646798194  1.0251965325
H -2.4962965690  1.0995651042 -1.2235898471
H -0.3419677267  2.0111640223 -1.9820697765
H  0.8092624913  2.4794431842 -0.7358347137
H -0.7640342381  3.2895905100 -0.8342945043
O  1.1998183627 -0.0000000000  0.0000000000
O -0.7276536286 -1.1221815998  0.0370887240
H -1.6622299740 -0.8263433184  0.0116700265
H -2.8791325705  1.5424501139  0.2989276277
```

Geometry-optimized zero-field structure of S-alanine (standard alignment, .xyz format)

```
13
geom opt E=-3.239066694749e+02 S-alanine
C -0.8414389890  1.2944103766  0.0000000000
C -0.2479078582  2.3365078003  0.9444013253
```

```
C  0.0000000000  0.0000000000  0.0000000000
N -2.2552642080  0.9681443632  0.2492518972
H -0.7691780585  1.6646798197 -1.0251965320
H -2.4962965699  1.0995651022  1.2235898462
H -0.3419677269  2.0111640204  1.9820697773
H  0.8092624905  2.4794431839  0.7358347145
H -0.7640342396  3.2895905087  0.8342945062
O  1.1998183626 -0.0000000000 -0.0000000000
O -0.7276536282 -1.1221816006 -0.0370887238
H -1.6622299737 -0.8263433197 -0.0116700274
H -2.8791325707  1.5424501135 -0.2989276284
```

Example of Gaussian input file for dihedral scan

Below is an example of a typical constrained optimization dihedral scan input file for Gaussian from a field-optimized starting structure. The structure of R-alanine, which has been geometry-optimized in an electric field of $+25x10^{-4}$ atomic units along C3-C10 in the x-axis direction, is set to have C1 (the conventional chiral center) at the origin and the C3-C10 bond distance is also constrained to its field-optimized value. The dihedral angle C3-C1-C2-H7 is then scanned for 180 steps of +1.0 degrees.

```
%NoSave
%mem=4GB
%nprocshared=4
%chk=alanine_R_Xplus25_3127_angleplus.chk
#p Opt(Modredundant,verytight,maxcycles=999) B3LYP/cc-pVTZ NoSymm Int(Grid=Ultrafine)
SCF(xqc,conver=12,maxcycle=999)

Dihedral scan C3-C1-C2-H7, step +1.0 degrees, bond length C3-C10 fixed

0 1
C  0.000000  0.000000  0.000000
C  0.588067  1.037607 -0.953610
C  0.841076 -1.294489  0.000000
N -1.413680 -0.332263 -0.237696
H  0.080102  0.376548  1.022987
H -1.671738 -0.185284 -1.206052
H  0.480592  0.710425 -1.990127
H  1.649197  1.173472 -0.755833
H  0.078376  1.994438 -0.841131
O  2.044830 -1.294489  0.000000
O  0.112508 -2.413312  0.035921
H -0.822901 -2.107076  0.008706
H -2.038244  0.221571  0.331707

X 1 F
B 3 10 F
D 3 1 2 7 S 180 1.0
```

Gaussian input template file for single-point wavefunctions

This single-point 'template' file is used (with the '**xyz_to_gjf**' program of QuantVec) to generate consistent single-point wavefunction jobs for all torsioned and untorsioned molecular geometries. The <**xyz**> tag in the template file is substituted with the actual molecular atomic coordinates.

```
%NoSave
%mem=4GB
%nprocshared=4
%chk=<name>.chk
#p B3LYP/cc-pVTZ NoSymm Int(Grid=Ultrafine) SCF(xqc,conver=12,maxcycle=999) Stable=Opt
Output=WFX

single point, stability checked

0 1
<xyz>

<name>.wfx
```

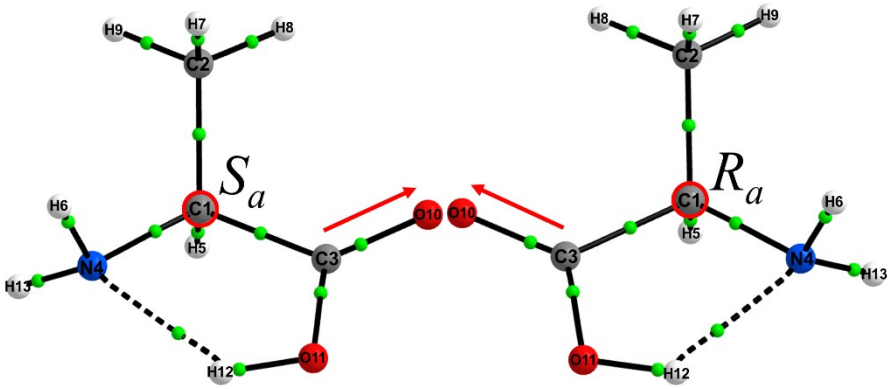

Scheme S6. Molecular graphs of the S_a stereoisomer (left panel) and R_a stereoisomer (right panel) of alanine, Note we use a subscript "a" and an italic font for the geometric stereoisomers because we have applied an **E**-field. The green spheres indicate the bond critical points (*BCP*s). The red arrows indicate the directions of the positive (+**E**) field along the C3→O10 *BCP* bond path and negative (-**E**) field along the C3←O10 *BCP* bond path. The C3, N4, and H5 atoms are bonded to the C1 atom; the H6, H7, and H8 atoms are bonded to the C2 atom. Numbered atoms in black define the dihedral angles {(3127, 3128, 3129), (4127, 4128, 4129), and (5127, 5128, 5129)} used in the construction of the spanning stress tensor trajectory $\mathsf{T}_{\boldsymbol{\sigma}}(s)$.

The effect of an applied electric field on the S_a and R_a geometric stereoisomers of alanine was determined and agreement with the CIP rules, see **Scheme S6**, **Figures S6(a-c)** and **Tables S6(a-d)**. There is a lack of mixing of the $\mathbf{S}_{\boldsymbol{\sigma}}$ and $\mathbf{R}_{\boldsymbol{\sigma}}$ chirality $\mathsf{C}_{\boldsymbol{\sigma}}$ assignments, i.e. $\mathsf{C}_{\boldsymbol{\sigma}\text{mixing}} = 0.0$ for $\mathbf{E} = \pm 25\times10^{-4}$ au, this indicates for $\mathbf{E} = \pm 25\times10^{-4}$ au that alanine possesses less achiral character compared with the absence of an **E**-field.

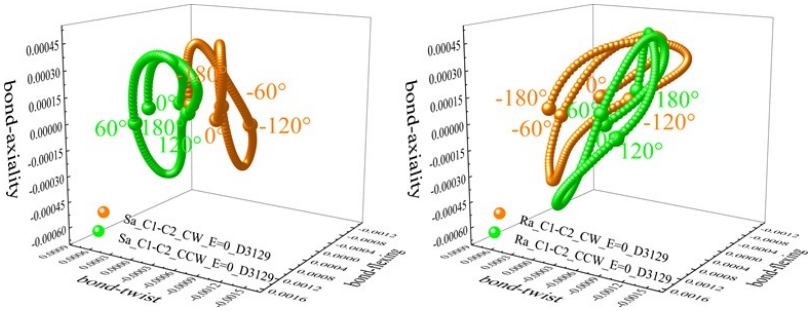

Figure S6(a). The stress tensor trajectory $\mathsf{T}_{\boldsymbol{\sigma}}(s)$ of the torsional C1-C2 *BCP* for the CW ($-90.0° \leq \theta \leq 0.0°$) and CCW ($0.0° \leq \theta \leq +90.0°$) directions corresponding to the D_{3129} dihedral angle for the **E**-field = 0. Left panel: the S_a stereoisomer; Right panel: the R_a stereoisomer. The degree markers for the torsion θ are indicated at steps of 30.0°.

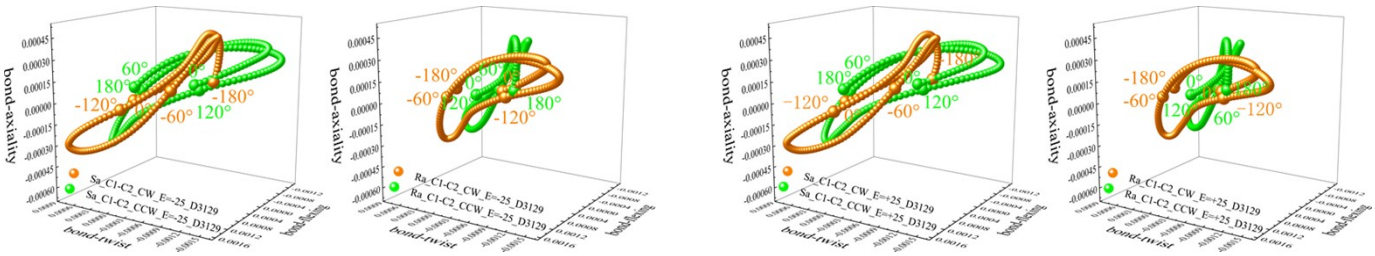

Figure S6(b). $\mathsf{T}_{\sigma}(s)$ of the torsional C1-C2 *BCP* bond path for the **E**-field = -25×10^{-4} a.u. (**a**) and $+25 \times 10^{-4}$ a.u. (**b**). $\mathsf{T}_{\sigma}(s)$ of the S_a and R_a stereoisomers are presented in the left and right panels.

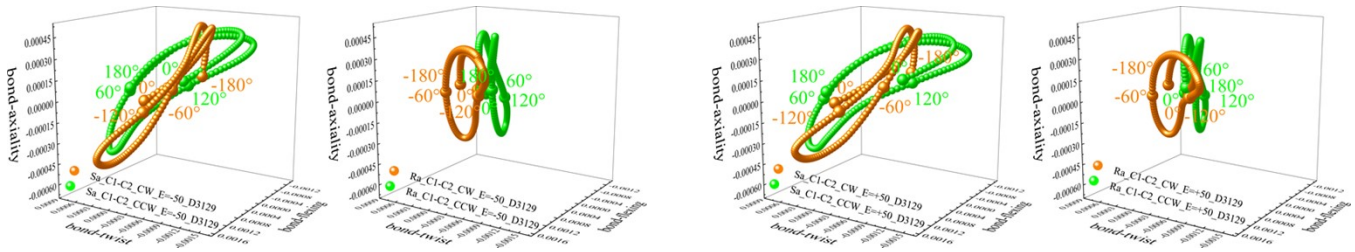

Figure S6(c). $\mathsf{T}_{\boldsymbol{\sigma}}(s)$ of the torsional C1-C2 *BCP* bond path for the **E** field = -50×10^{-4} a.u. (pair of left-panels) and $+50 \times 10^{-4}$ a.u. (pair of right-panels). $\mathsf{T}_{\boldsymbol{\sigma}}(s)$ of the S_a and R_a stereoisomers are presented in each of the pair the left and right panels.

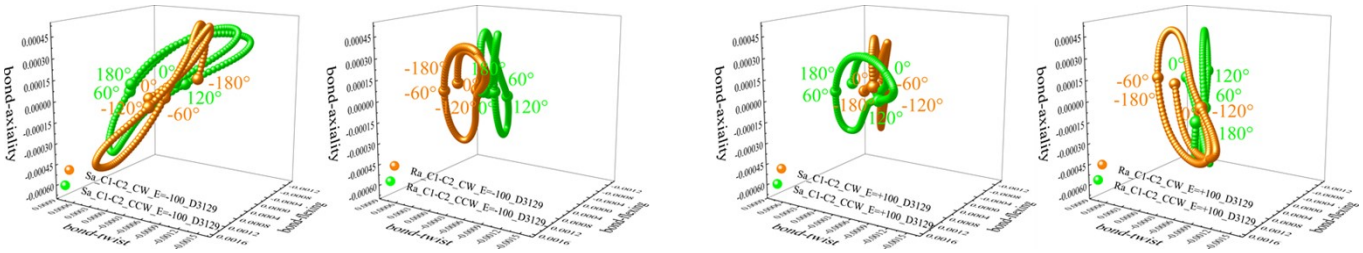

Figure S6(d). $\mathsf{T}_{\boldsymbol{\sigma}}(s)$ of the torsional C1-C2 *BCP* bond path for the **E** field = -100×10^{-4} a.u. (pair of left-panels) and $+100 \times 10^{-4}$ a.u. (pair of right-panels). $\mathsf{T}_{\boldsymbol{\sigma}}(s)$ of the S_a and R_a stereoisomers are presented in each of the pair the left and right panels.

Table S6(a). The maximum stress tensor projections {t_{1max} = bond-twist$_{max}$, t_{2max} = bond-flexing$_{max}$, t_{3max} =bond-axiality$_{max}$} for the dominant torsional C1-C2 *BCP* of alanine subjected to an electric field are presented; all entries have been multiplied by 10^3.

	{t_{1max} = bond-twist$_{max}$, t_{2max} = bond-flexing$_{max}$, t_{3max} =bond-axiality$_{max}$}			
	S_a		R_a	
	CW	**CCW**	**CW**	**CCW**
E-field =0 a.u				
D3127	{0.6556, 2.3194, 0.8907}	{1.4191, 1.5024, 0.8492}	{1.4203, 1.5024, 0.8492}	{0.6568, 2.3194, 0.8906}
D3128	{0.8060, 2.0810, 0.8903}	{0.9693, 1.7184, 0.8429}	{0.9693, 1.7186, 0.8429}	{0.8059, 2.0811, 0.8882}
D3129	{0.5524, 2.0338, 0.8893}	{1.4425, 1.5643, 0.8526}	{1.4425, 1.5643, 0.8526}	{0.5524, 2.0338, 0.8893}
D4127	{1.1338, 2.4641, 0.8995}	{1.6212, 2.1859, 0.8665}	{1.6212, 2.1858, 0.8664}	{1.1338, 2.4641, 0.8995}
D4128	{0.9248, 2.7882, 0.8950}	{1.6870, 1.9044, 0.8641}	{1.6873, 1.9040, 0.8641}	{0.9248, 2.7884, 0.8950}
D4129	{1.2886, 2.5276, 0.8884}	{1.3137, 2.2575, 0.8763}	{1.3139, 2.2575, 0.8763}	{1.2888, 2.5275, 0.8884}
D5127	{1.1089, 2.1614,0.8934}	{1.3127, 2.0045, 0.8624}	{1.3127, 2.0043, 0.8624}	{1.1087, 2.1611, 0.8935}
D5128	{1.1075, 2.3156, 0.8906}	{1.0125, 1.6827, 0.8590}	{1.0125, 1.6827, 0.8590}	{1.1076, 2.3155, 0.8906}
D5129	{0.5426, 2.0994, 0.8851}	{1.4648, 1.9453, 0.8680}	{1.4648, 1.9453, 0.8680}	{0.5426, 2.0995, 0.8851}
E-field = -25×10^{-4} a.u				
D3127	{2.2535, 1.6740, 0.8511}	{2.3675, 1.1764, 0.7867}	{2.3675, 1.1764, 0.7867}	{2.2546, 1.6740, 0.8511}
D3128	{2.1559, 1.3472, 0.8543}	{2.3594, 1.4102, 0.7799}	{2.3594, 1.4102, 0.7799}	{2.1561, 1.3470, 0.8546}
D3129	{1.8953, 1.6273, 0.8495}	{2.4999, 1.1390, 0.7890}	{2.4999, 1.1390,0.7889}	{1.8953, 1.6272, 0.8496}
D4127	{2.2993, 1.7907, 0.8594}	{2.9574, 1.2619, 0.8125}	{2.9573, 1.2619, 0.8123}	{2.2993, 1.7907, 0.8596}
D4128	{2.3108, 1.8682, 0.8600}	{2.7144, 1.2791, 0.8113}	{2.7144, 1.2812, 0.8114}	{2.3107, 1.8683, 0.8599}
D4129	{2.4497, 1.5733, 0.8511}	{2.5899, 1.4252, 0.8226}	{2.5899, 1.4252, 0.8227}	{2.4498, 1.5732, 0.8510}
D5127	{2.0336, 1.6815, 0.8549}	{2.2809, 1.6555, 0.8001}	{2.2808, 1.6556, 0.8001}	{2.0337, 1.6815, 0.8552}
D5128	{1.8926, 1.8082, 0.8553}	{2.0900, 1.3256, 0.7959}	{2.0899, 1.3257, 0.7959}	{1.8926, 1.8080, 0.8554}
D5129	{1.7494, 1.5733, 0.8476}	{2.1460, 1.6501, 0.8043}	{2.1459, 1.6501, 0.8043}	{1.7494, 1.5732, 0.8475}
E-field = -50×10^{-4} a.u				
D3127	{1.2033, 2.5396, 0.9214}	{1.5666, 2.0525, 0.8554}	{1.5668, 2.0524, 0.8554}	{1.2033, 2.5396, 0.9216}
D3128	{1.2766, 2.1749, 0.9259}	{1.2731, 2.3948, 0.8496}	{1.2730, 2.3948, 0.8496}	{1.2766, 2.1748, 0.9259}
D3129	{0.8865, 2.3385, 0.9181}	{1.6651, 2.1707, 0.8601}	{1.6650, 2.1708, 0.8601}	{0.8864, 2.3385, 0.9181}
D4127	{1.3023, 2.5612, 0.9276}	{1.8870, 2.5657, 0.8778}	{1.8868, 2.5659, 0.8776}	{1.3023, 2.5611, 0.9277}
D4128	{1.0520, 2.7841, 0.9291}	{1.9473, 2.3698, 0.8802}	{1.9473, 2.3697, 0.8802}	{1.0520, 2.7841, 0.9292}
D4129	{1.3473, 2.5898, 0.9178}	{1.5839, 2.4812, 0.8914}	{1.5839, 2.4811, 0.8914}	{1.3472, 2.5899, 0.9175}
D5127	{1.5348, 2.2073, 0.9245}	{1.4968, 2.3214, 0.8673}	{1.4968, 2.3213, 0.8673}	{1.5348, 2.2073, 0.9245}
D5128	{1.4765, 2.2625, 0.9265}	{1.2859, 2.1493, 0.8655}	{1.2859, 2.1494, 0.8656}	{1.4765, 2.2625, 0.9263}
D5129	{1.0246, 2.1667, 0.9158}	{1.6280, 2.2059, 0.8739}	{1.6281, 2.2060, 0.8738}	{1.0246, 2.1667, 0.9158}
E-field = -100×10^{-4} a.u				
D3127	{1.1857, 2.4683, 0.9403}	{1.5317, 1.9655, 0.8749}	{1.5316, 1.9655, 0.8749}	{1.1858, 2.4684, 0.9403}
D3128	{1.2468, 2.1547, 0.9448}	{1.2491, 2.3001, 0.8703}	{1.2491, 2.3001, 0.8703}	{1.2467, 2.1546, 0.9448}
D3129	{0.8828, 2.3097, 0.9361}	{1.6412, 2.0781, 0.8827}	{1.6410, 2.0779, 0.8829}	{0.8828, 2.3097, 0.9360}
D4127	{1.3362, 2.5354, 0.9456}	{1.8788, 2.5007, 0.8946}	{1.8787, 2.5007, 0.8947}	{1.3361, 2.5353, 0.9456}
D4128	{1.0886, 2.7521, 0.9480}	{1.9590, 2.2988, 0.8994}	{1.9590, 2.2988, 0.8995}	{1.0885, 2.7521, 0.9478}
D4129	{1.4070, 2.5672, 0.9335}	{1.5717, 2.4415, 0.9113}	{1.5717, 2.4416, 0.9113}	{1.4069, 2.5672, 0.9335}
D5127	{1.4972, 2.2190, 0.9434}	{1.4508, 2.2874, 0.8870}	{1.4507, 2.2873, 0.8869}	{1.4972, 2.2190, 0.9434}
D5128	{1.4312, 2.2578, 0.9453}	{1.2496, 2.0928, 0.8871}	{1.2496, 2.0929, 0.8871}	{1.4312, 2.2577, 0.9453}
D5129	{1.0010, 2.1477, 0.9333}	{1.5913, 2.1842, 0.8964}	{1.5913, 2.1841, 0.8964}	{1.0010, 2.1477, 0.9332}

E-field = +25×10^{-4} a.u

D3127	{2.1605, 1.9216, 0.8203}	{2.3480, 1.3947, 0.7569}	{2.3480, 1.3947, 0.7569}	{2.1603, 1.9215, 0.8204}
D3128	{2.1010, 1.5422, 0.8223}	{2.2974, 1.6772, 0.7516}	{2.2974, 1.6772, 0.7516}	{2.1011, 1.5423, 0.8224}
D3129	{1.7919, 1.8315, 0.8204}	{2.5131, 1.3838, 0.7571}	{2.5132, 1.3837, 0.7570}	{1.7920, 1.8315, 0.8204}
D4127	{2.1356, 1.9902, 0.8306}	{2.8429, 1.5258, 0.7889}	{2.8427, 1.5262, 0.7889}	{2.1342, 1.9884, 0.8300}
D4128	{2.1075, 2.1072, 0.8306}	{2.6537, 1.4992, 0.7839}	{2.6535, 1.4991, 0.7840}	{2.1076, 2.1071, 0.8306}
D4129	{2.2614, 1.8151, 0.8261}	{2.4947, 1.6505, 0.7948}	{2.4946, 1.6506, 0.7948}	{2.2613, 1.8151, 0.8261}
D5127	{2.0236, 1.8178, 0.8245}	{2.2300, 1.7500, 0.7710}	{2.2300, 1.7500, 0.7710}	{2.0236, 1.8179, 0.8244}
D5128	{1.8842, 1.9082, 0.8241}	{2.0021, 1.4855, 0.7658}	{2.0019, 1.4855, 0.7659}	{1.8842, 1.9083, 0.8241}
D5129	{1.6649, 1.7046, 0.8192}	{2.1289, 1.7371, 0.7724}	{2.1290, 1.7370, 0.7724}	{1.6649, 1.7046, 0.8192}

E-field = +50×10^{-4} a.u

D3127	{1.3830, 2.5990, 0.8623}	{1.7672, 2.0716, 0.7940}	{1.7673, 2.0716, 0.7939}	{1.3829, 2.5989, 0.8622}
D3128	{1.4581, 2.1575, 0.8643}	{1.4934, 2.4770, 0.7907}	{1.4934, 2.4770, 0.7908}	{1.4580, 2.1577, 0.8645}
D3129	{1.0333, 2.3712, 0.8622}	{1.9035, 2.2063, 0.7939}	{1.9033, 2.2061, 0.7940}	{1.0331, 2.3711, 0.8623}
D4127	{1.3528, 2.5576, 0.8699}	{2.0481, 2.5027, 0.8277}	{2.0485, 2.5027, 0.8275}	{1.3529, 2.5577, 0.8699}
D4128	{1.1266, 2.7698, 0.8712}	{2.0711, 2.3262, 0.8219}	{2.0712, 2.3262, 0.8220}	{1.1266, 2.7698, 0.8711}
D4129	{1.3764, 2.5515, 0.8675}	{1.7517, 2.4314, 0.8322}	{1.7518, 2.4313, 0.8323}	{1.3764, 2.5514, 0.8678}
D5127	{1.6817, 2.1896, 0.8653}	{1.6849, 2.2508, 0.8071}	{1.6848, 2.2507, 0.8072}	{1.6821, 2.1898, 0.8655}
D5128	{1.6251, 2.2263, 0.8655}	{1.4718, 2.1147, 0.8030}	{1.4718, 2.1147, 0.8031}	{1.6251, 2.2263, 0.8655}
D5129	{1.1684, 2.1223, 0.8607}	{1.8248, 2.1609, 0.8079}	{1.8248, 2.1610, 0.8080}	{1.1686, 2.1223, 0.8607}

E-field = +100×10^{-4} a.u

D3127	{1.5032,2.5241, 0.8241}	{1.9462, 2.0492, 0.7463}	{1.9462, 2.0492, 0.7462}	{1.5032,2.5242, 0.8242}
D3128	{1.5701, 2.0772, 0.8233}	{1.66432.44, 60, 0.7483}	{1.6645, 2.4462, 0.7483}	{1.5702, 2.0771, 0.8235}
D3129	{1.1415, 2.2724, 0.8230}	{2.0781, 2.1856, 0.7444}	{2.0780, 2.1856, 0.7445}	{1.1414, 2.2724, 0.8230}
D4127	{1.4386, 2.5202, 0.8266}	{2.1853, 2.4068, 0.7888}	{2.1851, 2.4066, 0.7888}	{1.4385, 2.5203, 0.8267}
D4128	{1.2461, 2.7011, 0.8295}	{2.1813, 2.2455, 0.7754}	{2.1812, 2.2454, 0.7753}	{1.2460, 2.7011, 0.8294}
D4129	{1.4467, 2.4553,0.8299}	{1.8801, 2.3656, 0.7860}	{1.8801, 2.3657, 0.7861}	{1.4468, 2.4552, 0.8298}
D5127	{1.7524, 2.1595, 0.8232}	{1.8480, 2.1928, 0.7590}	{1.8482, 2.1926, 0.7590}	{1.7528, 2.1596, 0.8233}
D5128	{1.6908, 2.1746, 0.8224}	{1.6019, 2.0552, 0.7538}	{1.6019, 2.0550, 0.7537}	{1.6907, 2.1746, 0.8223}
D5129	{1.2484, 2.0771, 0.8202}	{1.9637, 2.1080, 0.7564}	{1.9637, 2.1080, 0.7564}	{1.2482, 2.0770, 0.8204}

Table S6(b). The values of the chirality $C_\sigma = [(\mathbf{e_{1\sigma}\cdot dr})_{max}]_{CCW} - [(\mathbf{e_{1\sigma}\cdot dr})_{max}]_{CW}$, bond-flexing $F_\sigma = [(\mathbf{e_{2\sigma}\cdot dr})_{max}]_{CCW} - [(\mathbf{e_{2\sigma}\cdot dr})_{max}]_{CW}$, bond-axiality $B_\sigma = [(\mathbf{e_{3\sigma}\cdot dr})_{max}]_{CCW} - [(\mathbf{e_{3\sigma}\cdot dr})_{max}]_{CW}$ and the chirality-helicity function $C_{helicity} = C_\sigma|B_\sigma|$ of the torsional C1-C2 *BCP* of alanine are presented, all entries are multiplied by 10^3.

		S_a	
R_a			
C1-C2 *BCP*	$\{C_\sigma, F_\sigma, B_\sigma\}$	$C_{helicity}$ $[C_\sigma,\|B_\sigma\|]$	$\{C_\sigma, F_\sigma, B_\sigma\}$
E-field =0 a.u			
D3127	{0.7635**[S_σ]**, -0.8171**[R_σ]**, -0.0415**[R_σ]**}	1.1604**[S_σ, S_σ]**	{-0.7635**[R_σ]**,0.8170**[S_σ]**, 0.0414**[S_σ]**}
D3128	{0.1633**[S_σ]**, -0.3626**[R_σ]**, -0.0474**[R_σ]**}		{-0.1634**[R_σ]**, 0.3625**[S_σ]**, 0.0453**[S_σ]**}
D3129	{0.8901**[S_σ]**, -0.4695**[R_σ]**, -0.0367**[R_σ]**}		{-0.8901**[R_σ]**, 0.4694**[S_σ]**, 0.0367**[S_σ]**}
D4127	{0.4874**[S_σ]**, -0.2782**[R_σ]**, -0.0330**[R_σ]**}		{-0.4874**[R_σ]**, 0.2783**[S_σ]**, 0.0331**[S_σ]**}
D4128	{0.7623**[S_σ]**, -0.8838**[R_σ]**, -0.0309**[R_σ]**}		{-0.7624**[R_σ]**, 0.8844**[S_σ]**, 0.0309**[S_σ]**}
D4129	{0.0251**[S_σ]**, -0.2700**[R_σ]**, -0.0121**[R_σ]**}		{-0.0251**[R_σ]**, 0.2700**[S_σ]**, 0.0121**[S_σ]**}
D5127	{0.2039**[S_σ]**, -0.1569**[R_σ]**, -0.0310**[R_σ]**}		{-0.2040**[R_σ]**, 0.1568**[S_σ]**, 0.0311**[S_σ]**}
D5128	{-0.0950**[R_σ]** -0.6328**[R_σ]**, -0.0316**[R_σ]**}		{0.0951**[S_σ]**, 0.6328**[S_σ]**, 0.0316**[S_σ]**}
D5129	{0.9222**[S_σ]**, -0.1541**[R_σ]**, -0.0171**[R_σ]**}		{-0.9222**[R_σ]**, 0.1542**[S_σ]**, 0.0171**[S_σ]**}
E-field = -25×10^{-4} a.u			
D3127	{0.1140**[S_σ]**, -0.4976**[R_σ]**, -0.0644**[R_σ]**}	1.4262**[S_σ, S_σ]**	{-0.1129**[R_σ]**, 0.4976**[S_σ]**, 0.0644**[S_σ]**}
D3128	{0.2034**[S_σ]**, 0.0630**[S_σ]**, -0.0744**[R_σ]**}		{-0.2033**[R_σ]**, -0.0632**[R_σ]**, 0.0747**[S_σ]**}
D3129	{0.6046**[S_σ]**, -0.4883**[R_σ]**, -0.0605**[R_σ]**}		{-0.6046**[R_σ]**, 0.4882**[S_σ]**, 0.0606**[S_σ]**}
D4127	{0.6581**[S_σ]**, -0.5288**[R_σ]**, -0.0470**[R_σ]**}		{-0.6580**[R_σ]**, 0.5288**[S_σ]**, 0.0472**[S_σ]**}
D4128	{0.4036**[S_σ]**, -0.5891**[R_σ]**, -0.0487**[R_σ]**}		{-0.4037**[R_σ]**, 0.5871**[S_σ]**, 0.0485**[S_σ]**}
D4129	{0.1403**[S_σ]**, -0.1480**[R_σ]**, -0.0285**[R_σ]**}		{-0.1401**[R_σ]**, 0.1480**[S_σ]**, 0.0283**[S_σ]**}
D5127	{0.2472**[S_σ]**, -0.0260**[R_σ]**, -0.0549**[R_σ]**}		{-0.2471**[R_σ]**, 0.0259**[S_σ]**, 0.0552**[S_σ]**}
D5128	{0.1974**[S_σ]**, -0.4825**[R_σ]**, -0.0594**[R_σ]**}		{-0.1973**[R_σ]**, 0.4823**[S_σ]**, 0.0595**[S_σ]**}
D5129	{0.3965**[S_σ]**, 0.0769**[S_σ]**, -0.0433**[R_σ]**}		{-0.3965**[R_σ]**, -0.0769**[R_σ]**, 0.0432**[S_σ]**}
E-field = -50×10^{-4} a.u,			
D3127	{0.3633**[S_σ]**, -0.4871**[R_σ]**, -0.0660**[R_σ]**}	1.5676**[S_σ, S_σ]**	{-0.3635**[R_σ]**, 0.4872**[S_σ]**, 0.0662**[S_σ]**}
D3128	{-0.0034**[R_σ]**, 0.2199**[S_σ]**, -0.0763**[R_σ]**}		{0.0036**[S_σ]**, -0.2200**[R_σ]**, 0.0763**[S_σ]**}
D3129	{0.7787**[S_σ]**, -0.1677**[R_σ]**, -0.0580**[R_σ]**}		{-0.7786**[R_σ]**,0.1677**[S_σ]**, 0.0580**[S_σ]**}
D4127	{0.5847**[S_σ]**, 0.0046**[S_σ]**, -0.0498**[R_σ]**}		{-0.5845**[R_σ]**, -0.0048**[R_σ]**, 0.0501**[S_σ]**,
D4128	{0.8954**[S_σ]**, -0.4144**[R_σ]**, -0.0488**[R_σ]**}		{-0.8953**[R_σ]**, 0.4144**[S_σ]**, 0.0489**[S_σ]**}
D4129	{0.2366**[S_σ]**, -0.1085**[R_σ]**, -0.0263**[R_σ]**}		{-0.2367**[R_σ]**, 0.1088**[S_σ]**, 0.0261**[S_σ]**}
D5127	{-0.0381**[R_σ]**, 0.1141**[S_σ]**, -0.0572**[R_σ]**}		{0.0380**[S_σ]**, -0.1140**[R_σ]**, 0.0572**[S_σ]**}
D5128	{-0.1906**[R_σ]**, -0.1132**[R_σ]**, -0.0609**[R_σ]**}		{0.1906**[S_σ]**, 0.1131**[S_σ]**, 0.0607**[S_σ]**}
D5129	{0.6034**[S_σ]**, 0.0392**[S_σ]**, -0.0418**[R_σ]**}		{-0.6035**[R_σ]**, -0.0393**[R_σ]**, 0.0420**[S_σ]**}

E-field = -100×10^{-4} a.u{

D3127	{0.3460**[S_σ]**, -0.5028**[R_σ]**, -0.0654**[R_σ]**}	1.4209**[S_σ, S_σ]**	{-0.3458**[R_σ]**, 0.5029**[S_σ]**, 0.0655**[S_σ]**}
D3128	{0.0023**[S_σ]**,0.1454**[S_σ]**, -0.0744**[R_σ]**}		{-0.0023**[R_σ]**, -0.1455**[R_σ]**, 0.0744**[S_σ]**}
D3129	{0.7584**[S_σ]**, -0.2316**[R_σ]**, -0.0534**[R_σ]**}		{-0.7583**[R_σ]**, 0.2319**[S_σ]**, 0.0532**[S_σ]**}
D4127	{0.5426**[S_σ]**, -0.0347**[R_σ]**, -0.0510**[R_σ]**}		{-0.5427**[R_σ]**, 0.0346**[S_σ]**, 0.0509**[S_σ]**}
D4128	{0.8704**[S_σ]**, -0.4533**[R_σ]**, -0.0485**[R_σ]**}		{-0.8705**[R_σ]**, 0.4532**[S_σ]**, 0.0484**[S_σ]**}
D4129	{0.1647**[S_σ]**, -0.1257**[R_σ]**, -0.0221**[R_σ]**}		{-0.1648**[R_σ]**, 0.1256**[S_σ]**, 0.0222**[S_σ]**}
D5127	{-0.0464**[R_σ]**, 0.0684**[S_σ]**, -0.0565**[R_σ]**}		{0.0465**[S_σ]**, -0.0683**[R_σ]**, 0.0565**[S_σ]**}
D5128	{-0.1816**[R_σ]**, -0.1650**[R_σ]**, -0.0582**[R_σ]**}		{0.1816**[S_σ]**, 0.1648**[S_σ]**, 0.0582**[S_σ]**}
D5129	{0.5903**[S_σ]**, 0.0365**[S_σ]**, -0.0369**[R_σ]**}		{-0.5903**[R_σ]**, -0.0364**[R_σ]**, 0.0368**[S_σ]**}

E-field = +25×10^{-4} a.u

D3127	{0.1875**[S_σ]**, -0.5269**[R_σ]**, -0.0633**[R_σ]**}	1.6074**[S_σ, S_σ]**	{-0.1877**[R_σ]**, 0.5269**[S_σ]**, 0.0635**[S_σ]**}
D3128	{0.1964**[S_σ]**, 0.1349**[S_σ]**, -0.0707**[R_σ]**}		{-0.1964**[R_σ]**, -0.1349**[R_σ]**, 0.0708**[S_σ]**}
D3129	{0.7212**[S_σ]**, -0.4477**[R_σ]**, -0.0633**[R_σ]**}		{-0.7212**[R_σ]**, 0.4478**[S_σ]**, 0.0634**[S_σ]**}
D4127	{0.7072**[S_σ]**, -0.4645**[R_σ]**, -0.0417**[R_σ]**}		{-0.7085**[R_σ]**, 0.4622**[S_σ]**, 0.0411**[S_σ]**}
D4128	{0.5462**[S_σ]**, -0.6080**[R_σ]**, -0.0467**[R_σ]**}		{-0.5459**[R_σ]**, 0.6080**[S_σ]**, 0.0467**[S_σ]**}
D4129	{0.2333**[S_σ]**, -0.1645**[R_σ]**, -0.0313**[R_σ]**}		{-0.2333**[R_σ]**, 0.1646**[S_σ]**, 0.0313**[S_σ]**}
D5127	{0.2064**[S_σ]**, -0.0678**[R_σ]**, -0.0535**[R_σ]**}		{-0.2064**[R_σ]**, 0.0679**[S_σ]**, 0.0534**[S_σ]**}
D5128	{0.1179**[S_σ]**, -0.4227**[R_σ]**, -0.0583**[R_σ]**}		{-0.1177**[R_σ]**, 0.4228**[S_σ]**, 0.0582**[S_σ]**}
D5129	{0.4640**[S_σ]**, 0.0325**[S_σ]**, -0.0468**[R_σ]**}		{-0.4641**[R_σ]**, -0.0325**[R_σ]**, 0.0468**[S_σ]**}

E-field = +50×10^{-4} a.u

D3127	{0.3842**[S_σ]**, -0.5275**[R_σ]**, -0.0684**[R_σ]**}	1.9453**[S_σ, S_σ]**	{-0.3845**[R_σ]**, 0.5273**[S_σ]**, 0.0683**[S_σ]**}
D3128	{0.0353**[S_σ]**, 0.3194**[S_σ]**, -0.0735**[R_σ]**}		{-0.0354**[R_σ]**, -0.3193**[R_σ]**, 0.0737**[S_σ]**}
D3129	{0.8702**[S_σ]**, -0.1649**[R_σ]**, -0.0683**[R_σ]**}		{-0.8702**[R_σ]**, 0.1649**[S_σ]**, 0.0683**[S_σ]**}
D4127	{0.6954**[S_σ]**, -0.0549**[R_σ]**, -0.0423**[R_σ]**}		{-0.6957**[R_σ]**, 0.0550**[S_σ]**, 0.0425**[S_σ]**}
D4128	{0.9445**[S_σ]**, -0.4437**[R_σ]**, -0.0492**[R_σ]**}		{-0.9445**[R_σ]**, 0.4436**[S_σ]**, 0.0491**[S_σ]**}
D4129	{0.3754**[S_σ]**, -0.1201**[R_σ]**, -0.0353**[R_σ]**}		{-0.3754**[R_σ]**, 0.1201**[S_σ]**, 0.0355**[S_σ]**}
D5127	{0.0031**[S_σ]**, 0.0612**[S_σ]**, -0.0582**[R_σ]**}		{-0.0027**[R_σ]**, -0.0610**[R_σ]**, 0.0583**[S_σ]**}
D5128	{-0.1533**[R_σ]**, -0.1116**[R_σ]**, -0.0625**[R_σ]**}		{0.1533**[S_σ]**, 0.1116**[S_σ]**, 0.0624**[S_σ]**}
D5129	{0.6564**[S_σ]**, 0.0386**[S_σ]**, -0.0528**[R_σ]**}		{-0.6563**[R_σ]**, -0.0387**[R_σ]**, 0.0528**[S_σ]**}

E-field = +100×10^{-4} a.u

D3127	{0.4430**[S_σ]**, -0.4749**[R_σ]**, -0.0779**[R_σ]**}	2.4307**[S_σ, S_σ]**	{-0.4430**[R_σ]**, 0.4749**[S_σ]**, 0.0780**[S_σ]**}
D3128	{0.0942**[S_σ]**, 0.3688**[S_σ]**, -0.0750**[R_σ]**}		{-0.0942**[R_σ]**, -0.3690**[R_σ]**, 0.0752**[S_σ]**}
D3129	{0.9366**[S_σ]**, -0.0868**[R_σ]**, -0.0786**[R_σ]**}		{-0.9366**[R_σ]**, 0.0867**[S_σ]**, 0.0785**[S_σ]**}
D4127	{0.7467**[S_σ]**, -0.1135**[R_σ]**, -0.0378**[R_σ]**}		{-0.7466**[R_σ]**, 0.1137**[S_σ]**, 0.0379**[S_σ]**}
D4128	{0.9352**[S_σ]**, -0.4556**[R_σ]**, -0.0541**[R_σ]**}		{-0.9351**[R_σ]**, 0.4557**[S_σ]**, 0.0540**[S_σ]**}
D4129	{0.4333**[S_σ]**, -0.0896**[R_σ]**, -0.0438**[R_σ]**}		{-0.4333**[R_σ]**, 0.0895**[S_σ]**, 0.0437**[S_σ]**}
D5127	{0.0956**[S_σ]**, 0.0333**[S_σ]**, -0.0642**[R_σ]**}		{-0.0954**[R_σ]**, -0.0330**[R_σ]**, 0.0643**[S_σ]**}
D5128	{-0.0888**[R_σ]**, -0.1194**[R_σ]**, -0.0687**[R_σ]**}		{0.0887**[S_σ]**, 0.1195**[S_σ]**, 0.0686**[S_σ]**}
D5129	{0.7154**[S_σ]**, 0.0309**[S_σ]**, -0.0638**[R_σ]**}		{-0.7155**[R_σ]**, -0.0310**[R_σ]**, 0.0640**[S_σ]**}

Table S6(c). The variation of the distortion set ∑{chirality C_σ, bond-flexing F_σ, bond axiality B_σ} with the **E**-field×10^{-4} au of the $\mathbf{S}_\sigma$ and $\mathbf{R}_\sigma$ components for the S_a and R_a geometric stereoisomers. The sums of the corresponding mixing ratios are defined as $C_{\sigma mixing} = \sum_{S\sigma}\{C_\sigma\}/|\sum_{R\sigma}\{C_\sigma|$, $F_{\sigma mixing} = \sum_{S\sigma}\{F_\sigma\}/|\sum_{R\sigma}\{F_\sigma\}|$ and $B_{\sigma mixing} = \sum_{S\sigma}\{B_\sigma\}/|\sum_{R\sigma}\{B_\sigma\}|$.

	S_a	R_a			
(±)**E**-field	$\sum\{C_\sigma, F_\sigma, B_\sigma\}$	$\sum\{C_\sigma, F_\sigma, B_\sigma\}$	$C_{\sigma mixing}$	$F_{\sigma mixing}$	$B_{\sigma mixing}$
0	{4.1229[$\mathbf{S}_\sigma$], −4.0252[$\mathbf{R}_\sigma$], −0.2815[$\mathbf{R}_\sigma$]}	{−4.1230[$\mathbf{R}_\sigma$], 4.0254[$\mathbf{S}_\sigma$], 0.2792[$\mathbf{S}_\sigma$]}	0.0226	0.0000	0.0000
−25	{2.9650[$\mathbf{S}_\sigma$], −2.6204[$\mathbf{R}_\sigma$], −0.4810[$\mathbf{R}_\sigma$]}	{−2.9635[$\mathbf{R}_\sigma$], 2.6176[$\mathbf{S}_\sigma$], 0.4815[$\mathbf{S}_\sigma$]}	0.0000	0.0507	0.0000
−50	{3.2299[$\mathbf{S}_\sigma$], −0.9131[$\mathbf{R}_\sigma$], −0.4853[$\mathbf{R}_\sigma$]}	{−3.2299[$\mathbf{R}_\sigma$], 0.9131[$\mathbf{S}_\sigma$], 0.4855[$\mathbf{S}_\sigma$]}	0.0671	0.2927	0.0000
−100	{3.0467[$\mathbf{S}_\sigma$], −1.2629[$\mathbf{R}_\sigma$], −0.4664[$\mathbf{R}_\sigma$]}	{−3.0464[$\mathbf{R}_\sigma$], 1.2629[$\mathbf{S}_\sigma$], 0.4660[$\mathbf{S}_\sigma$]}	0.0697	0.1654	0.0000
+25	{3.3800[$\mathbf{S}_\sigma$], −2.5347[$\mathbf{R}_\sigma$], −0.4756[$\mathbf{R}_\sigma$]}	{−3.3812[$\mathbf{R}_\sigma$], 2.5328[$\mathbf{S}_\sigma$], 0.4752[$\mathbf{S}_\sigma$]}	0.0000	0.0619	0.0000
+50	{3.8112[$\mathbf{S}_\sigma$], −1.0034[$\mathbf{R}_\sigma$], −0.5104[$\mathbf{R}_\sigma$]}	{−3.8113[$\mathbf{R}_\sigma$], 1.0036[$\mathbf{S}_\sigma$], 0.5108[$\mathbf{S}_\sigma$]}	0.0387	0.2947	0.0000
+100	{4.3111[$\mathbf{S}_\sigma$], −0.9069[$\mathbf{R}_\sigma$], −0.5638[$\mathbf{R}_\sigma$]}	{−4.3111[$\mathbf{R}_\sigma$], 0.9071[$\mathbf{S}_\sigma$], 0.5642[$\mathbf{S}_\sigma$]}	0.0202	0.3232	0.0000

Table S6(d). The variation of the $\{C_\sigma, F_\sigma, B_\sigma\}$ with the ±**E**-field specified by the ratios $C_{\sigma E} = \sum\{C_\sigma\}/|\sum\{C_\sigma|_{E=0}$, $F_{\sigma E} = \sum\{F_\sigma\}/|\sum\{F_\sigma|_{E=0}$ and $B_{\sigma E} = \sum\{B_\sigma\}/|\sum\{B_\sigma|_{E=0}$ of the S_a and R_a geometric stereoisomers of alanine. The sum of the chirality-helicity function $\sum C_{helicity\mathbf{E}}$ is presented for the S stereoisomer. The $C_{helicity\mathbf{E}}$ is defined by the product $C_{\sigma E}|B_{\sigma E}|$, where the value of $\sum C_{helicity\mathbf{E}=0} = 1.1604$, i.e., in the absence of an **E**-field.

	S_a			R_a			
(±)**E**-field	$C_{\sigma E}$	$F_{\sigma E}$	$B_{\sigma E}$	$C_{\sigma E}$	$F_{\sigma E}$	$B_{\sigma E}$	$C_{helicity\mathbf{E}}$
−25	0.7192	0.6510	1.7087	0.7188	0.6503	1.7246	1.2291
−50	0.7834	0.2268	1.7240	0.7834	0.2268	1.7389	1.3509
−100	0.7390	0.3137	1.6568	0.7389	0.3137	1.6691	1.2245
+25	0.8198	0.6297	1.6895	0.8201	0.6292	1.7020	1.3852
+50	0.9244	0.2493	1.8131	0.9244	0.2493	1.8295	1.6764
+100	1.0456	0.2253	2.0028	1.0456	0.2253	2.0208	2.0947

7. Supplementary Materials S7. Full Symmetry-Breaking and Relevance for Stereochemistry: Why the *cis*-effect is the exception rather than the rule.

Here, as significant torsion of a 'double' bond is well known to lead to a multireference wavefunction, a Complete Active Space method with 2 electrons in 2 orbitals with Slater determinants is used for the CASSCF calculation. This CASSCF method for all single-point wavefunction calculations, geometry-optimization and constrained optimization dihedral scans in this work, for the ethene, its halogenated derivatives and the diazene N_2X_2 analogs.

Complete Active Space (CAS) geometry optimization of ethene

Below is a sample Gaussian input file for the initial geometry-optimization of ethene. The conventionally *cis* or *trans* halogen derivatives and the diazene N_2X_2 analogs are all geometry optimized using the same settings for method, convergence and basis set.

```
%NoSave
%mem=4GB
%nprocshared=4
%chk=ethene_geomopt.chk
#p Opt(verytight,maxcycles=999) CAS(2,2,SlaterDet) aug-cc-pVTZ NoSymm
Int(Grid=UltraFine) SCF(conver=12,maxcycle=999) Density=Current Freq Output=WFX

geom opt ethene cas(2,2)

0 1
C -0.000000  0.000000 -0.000000
C  1.321135  0.000000  0.000000
H -0.562872  0.913625  0.000000
H -0.562872 -0.913625  0.000000
H  1.884007 -0.913625 -0.000000
H  1.884007  0.913625  0.000000

ethene_geomopt.wfx
```

Dihedral scan of ethene and halogenated derivatives

Below is an example of a CAS(2,2) dihedral scan calculation input file using Gaussian, for the ethene molecule, used in this work. The dihedral scanned in this case is H3-C1-C2-H6 with steps of +1.0 degrees (all set on the last line of the file - the numbers after the 'D' are changed to scan other dihedral angles, or change the scan step to -1.0 degrees), using the converged geometry-optimized CAS(2,2) ethene structure as a starting structure, with the C1 atom at the origin, the C2 atom along the x-axis and atom number 3 in the x-y plane. The conventionally *cis* or *trans* halogen derivatives and the diazene N_2X_2 analogs are all dihedral-scanned using the same settings for method, convergence and basis set. In the case of the diazenes, there is only one possible choice of dihedral angle.

```
%NoSave
%mem=4GB
%nprocshared=4
%chk=ethene_3126_angleplus_cas.chk
#p   Opt(verytight,maxcycles=999,ModRedundant)   CAS(2,2,SlaterDet)   cc-pVTZ   NoSymm
Int(Grid=UltraFine) SCF(xqc,conver=12,maxcycle=999) Density=Current

CAS(2,2) cc-pVTZ SlaterDet scan plus

0 1
C  0.000000  0.000000  0.000000
C  1.333517  0.000000  0.000000
H -0.563067  0.914637  0.000000
H -0.563067 -0.914637  0.000000
H  1.896584 -0.914637  0.000000
H  1.896584  0.914637  0.000000

X 1 F
D 3 1 2 6 S 90 1.0
```

CAS(2,2) geometry optimized structures for ethene halogen derivatives and diazenes

Below are the additional CAS(2,2) geometry-optimized structures used, in **`.xyz`** format (Ångstrom units)

```
6
Cis-difluoroethene CAS(2,2) geometry optimized
C 0.0000000000 0.0000000000 0.0000000000
C 1.3235138900 -0.0000000000 -0.0000000000
F -0.7049023468 1.1131702584 0.0000000000
H -0.5783578339 -0.8986858780 -0.0000000337
H 1.9018717242 -0.8986858778 -0.0000000238
F 2.0284162368 1.1131702586 -0.0000000179

6
Trans-difluoroethene CAS(2,2) geometry optimized
C 0.0000000000 0.0000000000 0.0000000000
C 1.3231024961 -0.0000000000 0.0000000000
H -0.6166972691 0.8734323481 0.0000000000
F -0.6581584863 -1.1471189104 0.0000000045
H 1.9397997622 -0.8734323503 -0.0000000004
F 1.9812609847 1.1471189081 -0.0000000054

6
Cis-dichloroethene CAS(2,2) geometry optimized
C 0.0000000000 0.0000000000 0.0000000000
C 1.3275840786 0.0000000000 0.0000000000
Cl -0.9938039492 1.4065854239 0.0000000000
H -0.5415863730 -0.9217832279 -0.0000000069
H 1.8691704516 -0.9217832279 0.0000000041
```

Cl 2.3213880278 1.4065854239 -0.0000000268

6
Trans-dichloroethene CAS(2,2) geometry optimized
C 0.0000000000 0.0000000000 0.0000000000
C 1.3255411061 -0.0000000000 0.0000000000
H -0.5985438068 0.8846416889 -0.0000000000
Cl -0.8955809518 -1.4816308817 0.0000000051
H 1.9240849121 -0.8846416894 0.0000000014
Cl 2.2211220584 1.4816308810 -0.0000000022

4
Cis-N2H2 diazene CAS(2,2) geometry optimized
N 0.0000000000 0.0000000000 0.0000000000
N 1.2367424133 -0.0000000000 -0.0000000000
H -0.3878128704 0.9374428179 -0.0000000000
H 1.6245574260 0.9374419856 -0.0000004796

4
Trans-N2H2 diazene CAS(2,2) aug-cc-pVTZ geometry optimized
N 0.0000000000 0.0000000000 0.0000000000
N 1.2360751764 -0.0000000000 0.0000000000
H -0.3037408056 0.9640380580 0.0000000000
H 1.5398159305 -0.9640380739 -0.0000001484

4
Cis-N2F2 difluoroazene CAS(2,2) geometry optimized
N 0.0000000000 0.0000000000 0.0000000000
N 1.2157704749 0.0000000000 0.0000000000
F -0.5401037735 1.2120056725 0.0000000000
F 1.7558743404 1.2120061360 0.0000000000

4
Trans-N2F2 difluoroazene CAS(2,2) geometry optimized
N 0.0000000000 0.0000000000 0.0000000000
N 1.2152349472 0.0000000000 0.0000000000
F -0.3766507440 1.2740159183 0.0000000000
F 1.5918857986 -1.2740158930 0.0000000000

4
Cis-N2Cl2 dichloroazene CAS(2,2) geometry optimized
N 0.0000000000 0.0000000000 0.0000000000
N 1.2070260416 0.0000000000 0.0000000000
Cl -0.9015654100 1.4751311507 0.0000000000
Cl 2.1085889132 1.4751333847 0.0000000000

```
4
Trans-N2Cl2 dichloroazene CAS(2,2) geometry optimized
N 0.0000000000 0.0000000000 0.0000000000
N 1.2118269343 0.0000000000 0.0000000000
Cl -0.5911910867 1.6236941240 0.0000000000
Cl 1.8030180871 -1.6236941048 -0.0000016632
```

Single-point wavefunction calculation template input file

```
%NoSave
%mem=4GB
%nprocshared=4
%chk=<name>.chk
#p CAS(2,2,SlaterDet) cc-pVQZ NoSymm Int(Grid=UltraFine) SCF(conver=12,maxcycle=999)
Density=Current Output=WFX

single point CAS(2,2)

0 1
<xyz>

<name>.wfx
```

The *cis*-effect was found to be the exception rather than the rule that reflects the conventional energetics based understanding that steric effects are among the reasons for the differences between the relative energetic stabilities of *cis*- and *trans*-isomers, consistent with the previous association of chiral character in U_{σ}-space for the steric effects for ethane, **Table S7(a-c)** and **Figure 3** (Bottom)**.**

Table S7(a). The maximum stress tensor projections $T_{\sigma}(s)_{max}$ = {t_{1max} = bond-twist$_{max}$, t_{2max} = bond-flexing$_{max}$, t_{3max} =bond-axiality$_{max}$} of the torsion C1-C2 *BCP* of the unsubstituted and the doubly substituted ethene; all entries have been multiplied by 10^3.

	{t_{1max} = bond-twist$_{max}$, t_{2max} = bond-flexing$_{max}$, t_{3max} =bond-axiality$_{max}$}	
Isomer	**CW**	**CCW**
	***H*$_2$**	
D_{3125}	{0.421621, 1.749653, 0.538535}	{0.420658, 1.749885, 0.537814}
D_{3126}	{1.556154, 1.798145, 0.587711}	{1.556184, 1.798204, 0.587890}
D_{4125}	{1.582568, 1.807992, 0.595062}	{1.588166, 1.808127, 0.595067}
D_{4126}	{0.421531, 1.749428, 0.539150}	{0.421699, 1.749310, 0.538772}

	cis-ethene		*trans-ethene*	
	CW	**CCW**	**CW**	**CCW**
		***F*$_2$**		
D_{3125}	{0.894386, 2.478327, 0.766003}	{0.894951, 2.476430, 0.765981}	{0.633980, 1.614118, 0.490659}	{0.616676, 1.614120, 0.490754}
D_{3126}	{1.811066, 1.843635, 1.114622}	{1.797679, 1.843670, 1.113804}	{1.643756, 1.552269, 1.323383}	{1.644868, 1.552524, 1.323285}
D_{4125}	{1.379801, 1.681487, 0.853123}	{1.379820, 1.680001, 0.852128}	{1.346172, 2.036081, 0.453818}	{1.345872, 2.036362, 0.453826}
D_{4126}	{1.794181, 0.948874, 1.629433}	{1.795607, 0.947292, 1.628733}	{0.969545, 1.521856, 2.211110}	{0.968941, 1.521748, 2.211832}

Cl₂

D_{3125}	{0.730759, 2.389589, 0.394047}	{0.871561, 3.342181, 0.938698}	{0.269221, 1.876361, 0.289572}	{0.269308, 1.876577, 0.289551}
D_{3126}	{1.631687, 1.754600, 0.799802}	{1.630753, 1.755480, 0.799574}	{1.764909, 0.939509, 0.948342}	{1.360163, 1.133710, 1.085429}
D_{4125}	{1.598443, 1.390790, 0.802927}	{1.597514, 1.390777, 0.802122}	{1.896013, 2.115174, 0.184863}	{1.896178, 2.114261, 0.184909}
D_{4126}	{0.854010, 1.666286, 0.802408}	{0.466735, 1.778609, 0.336531}	{0.397264, 1.967998, 1.206856}	{0.397590, 1.968005, 1.206663}

Table S7(b). The maximum stress tensor projections $\mathsf{T}_{\sigma}(s)_{\max}$ = {$t_{1\max}$ = bond-twist$_{\max}$, $t_{2\max}$ = bond-flexing$_{\max}$, $t_{3\max}$ =bond-axiality$_{\max}$} of the torsion N1-N2 *BCP* of the doubly substituted diazene for the D_{3124} isomer; all entries have been multiplied by 10^3.

{$t_{1\max}$ = bond-twist$_{\max}$, $t_{2\max}$ = bond-flexing$_{\max}$, $t_{3\max}$ =bond-axiality$_{\max}$}

	cis-diazene		*trans-diazene*	
Isomer	**CW**	**CCW**	**CW**	**CCW**
		H₂		
	{4.801404, 2.787503, 5.635097}	{4.809519, 2.787666, 5.641851}	{4.856140, 3.448154, 5.073475}	{4.854382, 3.448856, 5.072910}
		F₂		
	{3.172154, 3.219492, 0.505581}	{3.161382, 3.210634, 0.508708}	{4.583991, 4.100396, 5.827743}	{4.584225, 4.100534, 5.827903}
		Cl₂		
	{1.475864, 1.395215, 0.849856}	{1.476064, 1.401934, 0.850026}	{25.90, 10.353290, 32.153236}	{25.904653, 10.349264, 31.819244}

Table S7(c). The ethene and doubly substituted ethene torsion C1-C2 *BCP* U_{σ}-space distortion sets {bond-twist T_{σ}, bond-flexing F_{σ}, bond-axiality B_{σ}} and sum of the four isomers: $\sum\{\mathsf{T}_{\sigma},\mathsf{F}_{\sigma},\mathsf{B}_{\sigma}\}$ for the *cis*- and *trans*-isomers. The four-digit sequence (left column) refers to the atom numbering sequence for the dihedral angles used to construct the $\mathsf{T}_{\sigma}(s)$, see **Figure 3** (Bottom) of the main text. The values of the total sums in the table correspond to all four isomers, the complete table for all four isomers (D_{3125}, D_{3126}, D_{4125}, D_{4126}), is provided.

H₂

D_{3125}	{-0.00096**[$\mathbf{R}_{\sigma}$]**, 0.00023**[$\mathbf{S}_{\sigma}$]**, -0.00072**[$\mathbf{R}_{\sigma}$]**}
D_{3126}	{0.00003**[$\mathbf{S}_{\sigma}$]**, 0.00006**[$\mathbf{S}_{\sigma}$]**, 0.00018**[$\mathbf{S}_{\sigma}$]**}
D_{4125}	{0.00560**[$\mathbf{S}_{\sigma}$]**, 0.00013**[$\mathbf{S}_{\sigma}$]**, 0.00001**[$\mathbf{S}_{\sigma}$]**}
D_{4126}	{0.00017**[$\mathbf{S}_{\sigma}$]**, -0.00012**[$\mathbf{R}_{\sigma}$]**, -0.00038**[$\mathbf{R}_{\sigma}$]**

$\sum\{\mathsf{T}_{\sigma}, \mathsf{F}_{\sigma}, \mathsf{B}_{\sigma}\}$

{0.00483**[$\mathbf{S}_{\sigma}$]**, 0.00030**[$\mathbf{S}_{\sigma}$]**, -0.00091**[$\mathbf{R}_{\sigma}$]**}

	cis-ethene $\{\mathsf{T}_{\sigma}, \mathsf{F}_{\sigma}, \mathsf{B}_{\sigma}\}$	*trans-ethene* $\{\mathsf{T}_{\sigma}, \mathsf{F}_{\sigma}, \mathsf{B}_{\sigma}\}$
	F₂	
D_{3125}	{0.00056**[$\mathbf{S}_{\sigma}$]**, -0.00190**[$\mathbf{R}_{\sigma}$]**, -0.00002**[$\mathbf{R}_{\sigma}$]**}	{-0.01731**[$\mathbf{R}_{\sigma}$]**, 0.00000**[$\mathbf{Q}_{\sigma}$]**, 0.00010**[$\mathbf{S}_{\sigma}$]**}
D_{3126}	{-0.01339**[$\mathbf{R}_{\sigma}$]**, 0.00004**[$\mathbf{S}_{\sigma}$]**, -0.00082**[$\mathbf{R}_{\sigma}$]**}	{0.00111**[$\mathbf{S}_{\sigma}$]**, 0.00026**[$\mathbf{S}_{\sigma}$]**, -0.00010**[$\mathbf{R}_{\sigma}$]**}
D_{4125}	{0.00002**[$\mathbf{S}_{\sigma}$]**, -0.00149**[$\mathbf{R}_{\sigma}$]**, -0.00100**[$\mathbf{R}_{\sigma}$]**}	{-0.00030**[$\mathbf{R}_{\sigma}$]**, 0.00028**[$\mathbf{S}_{\sigma}$]**, 0.00001**[$\mathbf{S}_{\sigma}$]**}
D_{4126}	{0.00143**[$\mathbf{S}_{\sigma}$]**, -0.00158**[$\mathbf{R}_{\sigma}$]**, -0.00070**[$\mathbf{R}_{\sigma}$]**}	{-0.00060**[$\mathbf{R}_{\sigma}$]**, -0.00011**[$\mathbf{R}_{\sigma}$]**, 0.00072**[$\mathbf{S}_{\sigma}$]**}
	$\sum\{\mathsf{T}_{\sigma}, \mathsf{F}_{\sigma}, \mathsf{B}_{\sigma}\}$	$\sum\{\mathsf{T}_{\sigma}, \mathsf{F}_{\sigma}, \mathsf{B}_{\sigma}\}$
	{-0.01138**[$\mathbf{R}_{\sigma}$]**, -0.00493**[$\mathbf{R}_{\sigma}$]**, -0.00253**[$\mathbf{R}_{\sigma}$]**}	{-0.01710**[$\mathbf{R}_{\sigma}$]**, 0.00043**[$\mathbf{S}_{\sigma}$]**, 0.00073**[$\mathbf{S}_{\sigma}$]**}
		Cl₂
D_{3125}	{0.14080**[$\mathbf{S}_{\sigma}$]**, 0.95259**[$\mathbf{S}_{\sigma}$]**, 0.54465**[$\mathbf{S}_{\sigma}$]**}	{0.00009**[$\mathbf{S}_{\sigma}$]**, 0.00022**[$\mathbf{S}_{\sigma}$]**, -0.00002**[$\mathbf{R}_{\sigma}$]**}
D_{3126}	{-0.00093**[$\mathbf{R}_{\sigma}$]**, 0.00088**[$\mathbf{S}_{\sigma}$]**, -0.00023**[$\mathbf{R}_{\sigma}$]**}	{-0.40475**[$\mathbf{R}_{\sigma}$]**, 0.19420**[$\mathbf{S}_{\sigma}$]**, 0.13709**[$\mathbf{S}_{\sigma}$]**}
D_{4125}	{-0.00093**[$\mathbf{R}_{\sigma}$]**, -0.00001**[$\mathbf{R}_{\sigma}$]**, -0.00081**[$\mathbf{R}_{\sigma}$]**}	{0.00017**[$\mathbf{S}_{\sigma}$]**, -0.00091**[$\mathbf{R}_{\sigma}$]**, 0.00005**[$\mathbf{S}_{\sigma}$]**}
D_{4126}	{-0.38727**[$\mathbf{R}_{\sigma}$]**, 0.11232**[$\mathbf{S}_{\sigma}$]**, -0.46588**[$\mathbf{R}_{\sigma}$]**}	{0.00033**[$\mathbf{S}_{\sigma}$]**, 0.00001**[$\mathbf{S}_{\sigma}$]**, -0.00019**[$\mathbf{R}_{\sigma}$]**}
	$\sum\{\mathsf{T}_{\sigma}, \mathsf{F}_{\sigma}, \mathsf{B}_{\sigma}\}$	$\sum\{\mathsf{T}_{\sigma}, \mathsf{F}_{\sigma}, \mathsf{B}_{\sigma}\}$
	{-0.24833**[$\mathbf{R}_{\sigma}$]**, 1.06578**[$\mathbf{S}_{\sigma}$]**, 0.07774**[$\mathbf{S}_{\sigma}$]**}	{-0.40417**[$\mathbf{R}_{\sigma}$]**, 0.19351**[$\mathbf{S}_{\sigma}$]**, 0.13692**[$\mathbf{S}_{\sigma}$]**}

Table S7(d). Summary comprising the ∑{bond-twist T_σ, bond-flexing F_σ} of the torsion C1-C2 *BCP* of ethene and the *cis*- and *trans*-isomers of doubly substituted ethene and the corresponding results for diazene, see **Figure 3** (Bottom) for the corresponding trajectories $\mathsf{T}_\sigma(s)$.

	$\sum\{\mathsf{T}_\sigma, \mathsf{F}_\sigma\}$	
H_2-ethene	{0.00483[$\mathbf{S}_\sigma$], 0.00030[$\mathbf{S}_\sigma$]}	
	cis-ethene	*trans*-ethene
	$\sum\{\mathsf{T}_\sigma, \mathsf{F}_\sigma\}$	$\sum\{\mathsf{T}_\sigma, \mathsf{F}_\sigma\}$
F_2-ethene	{-0.01138[$\mathbf{R}_\sigma$], -0.00493[$\mathbf{R}_\sigma$]}	{-0.01710[$\mathbf{R}_\sigma$], 0.00043[$\mathbf{S}_\sigma$]}
Cl_2-ethene	{-0.24833[$\mathbf{R}_\sigma$], 1.06578[$\mathbf{S}_\sigma$]}	{-0.40417[$\mathbf{R}_\sigma$], 0.19351[$\mathbf{S}_\sigma$]}
	$\{\mathsf{T}_\sigma, \mathsf{F}_\sigma\}$	$\{\mathsf{T}_\sigma, \mathsf{F}_\sigma\}$
H_2-diazene	{0.00812[$\mathbf{S}_\sigma$], 0.00016[$\mathbf{S}_\sigma$]}	{-0.00176[$\mathbf{R}_\sigma$]}, {0.00070[[$\mathbf{S}_\sigma$]}
F_2-diazene	{-0.01077**[**$\mathbf{R}_\sigma$], -0.00886**[**$\mathbf{R}_\sigma$]}	{0.00023[$\mathbf{S}_\sigma$]}, {0.00014 [$\mathbf{S}_\sigma$]}
Cl_2-diazene	{0.00020[$\mathbf{S}_\sigma$], 0.00672[$\mathbf{S}_\sigma$]}	{-0.00022 $\mathbf{R}_\sigma$]}, {-0.00402 **[**$\mathbf{R}_\sigma$]}

References

1 R. F. W. Bader, *J. Phys. Chem. A*, 1998, **102**, 7314–7323.
2 R. F. W. Bader, *J. Phys. Chem. A*, 2009, **113**, 10391–10396.
3 H. Nakatsuji, *J. Am. Chem. Soc.*, 1974, **96**, 24–30.
4 R. G. A. Bone and R. F. W. Bader, *J. Phys. Chem.*, 1996, **100**, 10892–10911.
5 S. Jenkins and M. I. Heggie, *J. Phys. Condens. Matter*, 2000, **12**, 10325–10333.
6 P. W. Ayers and S. Jenkins, *J. Chem. Phys.*, 2009, **130**, 154104.
7 S. Jenkins and I. Morrison, *Chem. Phys. Lett.*, 2000, **317**, 97–102.
8 S. Jenkins, J. R. Maza, T. Xu, D. Jiajun and S. R. Kirk, *Int. J. Quantum Chem.*, 2015, **115**, 1678–1690.
9 R. F. W. Bader, *J. Chem. Phys.*, 1980, **73**, 2871–2883.
10 R. E. Wyatt, *Quantum Dynamics with Trajectories*, Springer, Dordrecht, 1st edn., 2006.
11 P. Szarek, Y. Sueda and A. Tachibana, *J. Chem. Phys.*, 2008, **129**, 094102.
12 Z. Li, X. Nie, T. Xu, S. Li, Y. Yang, H. Früchtl, T. van Mourik, S. R. Kirk, M. J. Paterson, Y. Shigeta and S. Jenkins, *Int. J. Quantum Chem.*, 2021, **121**, e26793.
13 T. Tian, T. Xu, S. R. Kirk, I. T. Rongde, Y. B. Tan, S. Manzhos, Y. Shigeta and S. Jenkins, *Phys. Chem. Chem. Phys.*, 2020, **22**, 2509–2520.
14 W. Yang and I. Zurbenko, *Wiley Interdiscip. Rev. Comput. Stat.*, 2010, **2**, 340–351.
15 I. S. Ufimtsev and T. J. Martinez, *J. Chem. Theory Comput.*, 2009, **5**, 2619–2628.
16 I. S. Ufimtsev and T. J. Martinez, *J. Chem. Theory Comput.*, 2009, **5**, 1004–1015.
17 I. S. Ufimtsev and T. J. Martínez, *J. Chem. Theory Comput.*, 2008, **4**, 222–231.
18 S. Seritan, C. Bannwarth, B. S. Fales, E. G. Hohenstein, C. M. Isborn, S. I. L. Kokkila-Schumacher, X. Li, F. Liu, N. Luehr, J. W. Snyder Jr., C. Song, A. V. Titov, I. S. Ufimtsev, L.-P. Wang and T. J. Martínez, *WIREs Comput. Mol. Sci.*, 2021, **11**, e1494.
19 W. Zou, Molden2AIM (version 5.0.6) https://github.com/zorkzou/Molden2AIM 2021.
20 A. Nikiforov, J. A. Gamez, W. Thiel and M. Filatov, *J. Phys. Chem. Lett.*, 2016, **7**, 105–110.
21 L. Wang, G. Huan, R. Momen, A. Azizi, T. Xu, S. R. Kirk, M. Filatov and S. Jenkins, *J. Phys. Chem. A*, 2017, **121**, 4778–4792.
22 L. Wang, A. Azizi, R. Momen, T. Xu, S. R. Kirk, M. Filatov and S. Jenkins, *Int. J. Quantum Chem.*, 2020, **120**, e26062.
23 T. Xu, J. H. Li, R. Momen, W. J. Huang, S. R. Kirk, Y. Shigeta and S. Jenkins, *J. Am. Chem. Soc.*, 2019,

141, 5497–5503.
24 J. D. Hunter, *Comput. Sci. Eng.*, 2007, **9**, 90–95.